THE EFFECTS OF DEPOSITION PARAMETERS ON HYDROGENATED AMORPHOUS SILICON FILMS FABRICATED BY MICROWAVE GLOW DISCHARGE TECHNIQUES

by

Sergio Ruperto Tadeo Mejia Zenteno

A thesis
presented to the University of Manitoba
in partial fulfillment of the
requirements for the degree of
Master of Science
in
Electrical Engineering

Winnipeg, Manitoba, 1983

THE EFFECTS OF DEPOSITION PARAMETERS ON HYDROGENATED AMORPHOUS SILICON FILMS FABRICATED BY MICROWAVE GLOW DISCHARGE TECHNIQUES

by

Sergio Ruperto Tadeo Mejia Zenteno

A thesis submitted to the Faculty of Graduate Studies of the University of Manitoba in partial fulfillment of the requirements of the degree of

MASTER OF SCIENCE

ABSTRACT

Hydrogenated amorphous silicon (a-Si:H) films have been fabricated by a novel method of microwave glow-discharge deposition, operating at 2.45 GHz. The properties of these films, including dark conductivity, photoconductivity, optical constants, the optical gap, and the B value (gradient of $(\alpha\hbar\nu)^{1/2}$ versus $\hbar\nu$), have been measured and used to characterize their electronic structure. It has been found that the quality of the films depends strongly upon the microwave power density in the glow discharge, the confinement of the plasma, the position of the substrates relative to the plasma region, and the orientation of the electric field vector of the guided microwave radiation. The material is also strongly affected by the substrate temperature and the hydrogen content in the gas mixture of SiH_4, Ar, and H_2, as with films prepared by conventional techniques. Analysis of infrared absorption data and of impurity content by energy dispersive x-ray analysis indicates that by reducing the microwave power density and by properly confining the plasma in an isolated region by means of a magnetic field, the impurity contamination can be reduced to an insignificant level. Scanning electron microscopy reveals that the morphological structure of the films is associated with the

direction of the electric field vector and the power density of the guided microwave radiation. The deposition rate by the microwave glow-discharge method is generally higher than that by radio frequency glow discharge, for the same power density. The microwave techniques may prove to be more efficient than conventional rf or dc techniques for the fabrication of amorphous semiconductors films, provided that the deposition parameters can be equally well controlled.

ACKNOWLEDGEMENTS

Many thanks to my thesis advisor, Professor K.C. Kao, for suggesting this thesis subject, and for his constant encouragement, advice, and supervision.

Sincere thanks are given to the graduate students of the Materials and Devices Research Laboratory and the staff of the Electrical Engineering Department of the University of Manitoba for their assistance, co-operation, and understanding.

Special thanks and acknowledgements to Professor H.C. Card for his constant advice and encouragement, and to my colleague R.D. McLeod with whom I shared an important part of this experimental work and a good deal of helpful discussion.

TABLE OF CONTENTS

LIST OF FIGURES

Chapter I

INTRODUCTION.

Thin film fabrication utilizing low pressure chemical vapor deposition (CVD) promoted by a glow discharge, which is also known as plasma enhanced chemical vapor deposition (PECVD), has been used in recent years in research laboratories as well as in factories in the fields of microelectronics, optics, and photovoltaic devices. In particular in the area of photovoltaic devices amorphous hydrogenated silicon alloys (a-Si:H) have been found to have remarkable properties suitable for solar cells, which can be fabricated by this technique on inexpensive substrates at low cost. At the present time the energy conversion efficiency of amorphous silicon solar cells has reached approximately 10 %, which is comparable to the average efficiency of 14% for single-crystal silicon solar cells, but the fabrication cost for the latter is much higher.

PECVD is a complex process and it is still not well understood. However, its wide use for thin film fabrication has stimulated the research towards the understanding of this technique. There are several PECVD parameters that are known to affect the film properties such as the plasma power, gas pressure, gas flow, reactant concentrations, etc.

Present commercial PECVD systems, such as those used in silicon integrated circuit processing, are mainly of the Reinberg radial flow type operating at a frequency of 13.6 MHz. It should be noted that the effect of the frequency of the electromagnetic excitation of the plasma on the film properties is unknown and very little information is available in the literature about PECVD operating at frequencies in the 50 MHz to microwave range. This may be due to the fact that variable-frequency power supplies are not common. It is possible that the deposition process may be quite different if PECVD is conducted at high frequencies, particularly at frequencies much greater than the electron collision rate, since the relaxation processes can no longer follow the field.

The main purpose of the investigation being reported in this thesis is to study the feasibility of fabricating a-Si:H thin films, and other semiconductor alloy films such as $Si_{1-x}Ge_x$, $Si_{1-x}N_x$, $Si_{1-x}C_x$, etc. by microwave PECVD. In such a multidisciplinary subject it is important to understand the phenomena of glow discharge, and thus, a brief review of glow discharge concepts is given in Chapter II. In this chapter also are described various fabrication techniques used for solid thin film deposition including the fabrication parameters that control the electronic and optical properties of amorphous silicon films. The design, construction, and operation of three configurations of the microwave

PECVD systems are described in Chapter III; and the film characterization techniques, the optical, electronic, and morphological properties of the films, and the comparison of our results with those of other investigators in Chapter IV. Conclusions and recommendations for further work are given in Chapter V.

Chapter II

PLASMA PROPERTIES AND FABRICATION TECHNIQUES.

2.1 GLOW DISCHARGE AND PLASMA PARAMETERS [7,15,17,31].

Practical glow discharge such as that used in sputtering and PECVD is a very complicated environment containing electrons, various types of ions, neutral atoms and molecules, and photons. They are not necesarily homogeneous, with well defined potential and density, and their constituents are under non-equilibrium conditions. Nevertheless, the glow discharge can be studied, in a first approximation, by considering it a simplified Lorentz plasma. In a Lorentz plasma it is assumed that the electrons interact with each other only through collective spacecharge forces, and that the heavy positive ions and neutral molecules are at rest. In particular, in the so called "cold plasma", the effects which depend on the electron temperature are neglected first, and latter added as small corrections to the effective plasma parameters. A simplified glow discharge plasma consists of positive ions and negative electrons, and mainly un-ionized neutral molecules having a degree of ionization of 10^{-4} , so that essentially it still is a neutral gas that can be described by the gas laws. The prime feature of such a discharge is the ionization process which produces as many

as 10^{18} electron-ion pairs per cm^3 per second mainly by collisions. In the actual plasma the collision processes involve collisions between all possible species but electrons are the dominant species in determining the macroscopic behaviour of the glow discharge.

2.1.1 Collision processes [7,17,31].

Collision processes can be broadly divided into elastic and inelastic collisions, according to whether the internal (potential) energies of the colliding particles are conserved. The internal energy may be in the form of electronic excitation, ionization, etc. An elastic collision involves only the interchange of kinetic energy, while an inelastic collision involves changes in both kinetic and internal energies.

On the assumption that a large particle of mass M is initially at rest, and a small particle of mass m collides with M at a velocity v forming an angle ϕ with the line joining the centers of m and M at the moment of collision, and that the collision is elastic (no change in potential energies); then from the conservation of linear momentum and energy, the fractional energy transfer (FET) from mass m to mass M is given by

$$FET = [4\ m\ M\ /(m+M)^2]\ \cos^2\phi \qquad (2.1)$$

The FET function has a maximum value of $\cos\phi$ when m = M, that is for collisions between the same species in the medium. This is why the speed of 90% of gas atoms in the steady state conditions is within a factor of two of the mean speed. This also implies that when the masses of the colliding particles are very much different, such as in the case of an electron and a gas atom, very little energy can be transfered. Another interesting implication from the FET function is that when M>>m in a head on collision (ϕ=0), the FET becomes 4m/M. This means that the lighter particle speeds away at a speed twice the impact velocity. If the collision is inelastic, the particle will gain an internal energy ΔU. Using similar linear momentum and energy conservation conditions, the maximum of the FET for the transfer of kinetic energy to internal energy, can be expressed as

$$(FET)_{max} = \Delta U / [(1/2)\, mv^2] = [\, M /(m+M)]\, \cos^2\phi \qquad (2.2)$$

This indicates that when m<<M the inelastic energy transfer function can reach unity. This case corresponds to the case of collision between an electron and a gas atom or molecule, where a very efficient energy transfer may take place.

An electron approaching an atom sees the atom as an assembly of electrons and ions in largely empty space. The interaction between the primary electron and the electrons and

ions of the atom takes place under strong electrostatic forces, so that the precise outcome depends on the details of the approach of the electron, which introduces an element of probability or uncertainty into the interaction. This probability can be taken into account by means of its relation to a collision cross-section, q , for the event. In classical gas discharge terminology, it is customary to define a normalized probability of collision, P_c, as the average number of collisions which an electron makes in travelling one centimeter through a gas at 1 torr pressure and at 0 °C. If there are N atoms per cubic centimeter, then we have

$$N\,q = p_o P_c \tag{2.3}$$

where p is the reduced pressure given by $p_o = 273p/T$. The mean free path, l_c, is the average distance over which a particle travels between collisions with atoms. The relation between l_c and P_c is

$$l_c = 1/p_o P_c \tag{2.4}$$

The collision frequency, ν_c , is the average number of collisions which a gas atom makes per unit time. It is given by

$$\nu_c = p_o P_c v = N\,q\,v \tag{2.5}$$

For inelastic collisions, such as ionization, excitation, and dissociation, it is also possible to describe them in terms of cross sections. The total effective cross-section q can be defined as

$$q = q_o + \Sigma q_n \tag{2.6}$$

where q_o and q_n are, respectively, the cross-sections for elastic and inelastic types of collisions.

The over-all collision frequency is the sum of the component collision frequencies for each relevant process.

$$\nu_c = n_1 q_1 v + n_2 q_2 v + \ldots = \nu_1 + \nu_2 + \ldots \tag{2.7}$$

The collision frequency increases with increasing cross section. Thus, for instance, collisions with impurity particles having a large cross-section q may contribute significantly to the over-all collision frequency even though they are present in a small concentration n. Since the interaction time in a collision process decreases with increasing velocity, the cross section is velocity dependent. Furthermore, the situation is complicated by resonance and quantum mechanical effects. Thus, it is necessary, in general, to resort to experiment to determine cross-sections empirically, including the dependence on electron velocity and on scattering angle. Thus far, monoenergetic particles have

been assumed. If they follow some form of velocity distribution, not necessarily Maxwellian, the cross sections and collision frequencies must be appropriately averaged over all velocities.

Ionization. Among the inelastic collisions, electron impact ionization is the most important process in sustaining the glow discharge. In electron impact ionization a primary electron removes an electron from the atom, producing a positive ion and an additional electron following the reaction

$$e + Ar \longrightarrow 2\,e + Ar^{+} \qquad (2.8)$$

These two electrons are then accelerated by the electric field until they, too, can produce ionization. It is by this multiplication process that a glow discharge is maintained. The minimum energy required to remove the most weakly bound electron from the atom is known as the ionization potential, E_i. Below this threshold the ionization cross section for this process is zero, but increases almost linearly at first, and then gradually with electron energy up to about 100 eV, and then tends to fall off for higher energies.

Photoionization. A molecule or an atom in a ground state can be ionized by a photon provided its energy is equal or greater than the ionization potential.

Excitation. An electron can make only elastic collisions with a gas atom when its energy is insufficient to excite

any level characteristic of the target atom. As with ionization, there is a minimum energy for the occurrence of excitation. For example, the first excitation potential of Ar is 11.56 eV, and the cross section of the 2p level goes through a maximum at 21 eV. The cross section of molecules has a lower threshold for excitation than the corresponding atoms because of the possibilities of vibrational and rotational excitation. As with ionization, excitation can also be caused by photons. Some excited atoms have very long lifetimes (e.g. 1 msec to 1 sec) and these are known as metastable excited atoms; they arise because the selection rules forbid them to relax to their ground state; this means that the probability of such a transition is small. Argon has metastables at 11.5 eV and 11.7 eV.

Relaxation. The excited atoms and molecules are rather unstable and the electron configuration in the excited states soon returns to its original (ground) state in one or several transitions, with lifetimes varying from nanoseconds to seconds. Each transition is accompanied by the emission of a photon of very specific energy, equal to the difference in energy between the relevant quantum levels. This process of de-excitation of electronically excited atoms and molecules is called relaxation. The energy difference is characteristic of the transition in the atom or molecule, and constitutes a finger-print of the constituent species in the plasma. This has been used as the basis of a very useful

technique for plasma diagnosis called "Optical Emission Spectroscopy" (OES). With suitable detection equipment it is possible to detect photons from deep ultraviolet (atomic transitions) to far infra-red (molecular vibrational and rotational transitions).

Ionization from metastable states. Ionization can also be produced by an electron with energy less than the ionization energy, in collision with a molecule which has already been raised to an excited state E_e . This ionization can occur when

$$(1/2)mv^2 > E_i - E_e \qquad (2.9)$$

In fact, the chance of ionization from a metastable state by a favorable collision is greater because of the relatively long lifetime of metastable states compared with that of other excited states.

Considering the 11.55 eV metastable in argon, the threshold for ionization of this metastable would be only 4.21 eV, compared to 15.76 eV for the ground state argon atom. Although there usually are much fewer metastables than ground state atoms in a glow discharge, there are many more electrons capable of ionizing the metastables than those capable of ionizing the ground state atoms. Even though very little is known about the cross section of the metastable, it might well have a much larger cross section than its

ground state atom; this could make the ionization of the metastable comparable to that of ground states for electron energies of 2-4 eV. Thus, we can consider the glow discharge as a source of ion-electron pairs.

$$e + Ar^* \longrightarrow Ar^+ + 2\,e \qquad (2.10)$$

Two other possible ionization processes involving metastables are the collision of the metastables with ground state atoms and with other metastables, such as

$$A^* + B \longrightarrow B^+ + A + e \qquad (2.11)$$

(Penning ionization)

$$Ar^* + Ar^* \longrightarrow Ar + Ar^+ + e \qquad (2.12)$$

Dissociation. Dissociation of molecules can in principle be accomplished by an electron impact with any energy in excess of the dissociation threshold, i.e. the relevant bond strength in the molecule. In the glow discharge, electron impact dissociation is common:

$$e + O_2 \longrightarrow e + O + O \qquad (2.13)$$

A normal result of dissociation is an enhancement of chemical activity since the products are usually more reactive

than the parent molecule. Dissociation may also be accompanied by ionization:

$$e + CF_4 \text{ ---> } 2e + CF_3^+ + F \qquad (2.14)$$

Electron attachment. An electron may collide with an atom and then attach to it to form a negative ion. This process is refered to as the "electron attachment". Inert gas atoms have only filled outer electron shells, and so have little or no propensity to form negative ions. But halogens or oxygen atoms have high electron affinities and so readily form negative ions. Sometimes, electron attachment leads to dissociation and the process is called the "dissociative attachment".

$$e + O_2 \text{ ----> } O^- + O \qquad (2.15)$$

Ion neutral collisions. If the interaction between an ion and an atom takes place slowly, the internal motion of the system can gradually adjust itself throughout the collision without any energy transition occurring and such a collision is elastic. But, if the collision is very rapid, an inelastic collision will occur resulting in radiation or ionization. Charge transfer between ions moving in parent atoms or molecules is called "symmetrical resonant charge transfer",

and is rather unimportant since it involves only a momentum exchange. Charge exchange between unlike systems, called the "asymmetric charge transfer", could be more important, but tends to be less efficient. Both charge transfer processes contribute to the change of the energy distribution of ions and neutrals.

$$B^+ + C \text{ ----> } B + C^+ \qquad (2.16)$$

Recombination. In a gas containing positive ions and electrons, there is a tendency for these to come together in collision and recombine to form neutral atoms. But a two body recombination is very unlikely as it can be shown by momentum and energy conservation that yields an imaginary solution for the speed of the newly formed atom. A third body must take part to allow the recombination process to simultaneously satisfy the conservation requirements of energy and momentum. The third body is often a wall or may be another gas atom. As a result, there is, in general, little recombination in the body of the gas at low pressure. The kinetic energy loss of the electron may be emitted as a quantum of radiation (radiative recombination), but the probability of such emission is low.

2.1.2 Plasma parameters [7,15,17].

The principal mechanisms in the plasma are excitation, relaxation, ionization, and recombination. When a steady state is reached, there is an equilibrium between the rate of formation of ions and the rate of their recombination. This implies that an external energy source is required to maintain the dynamic equilibrium. In practice, such an energy source is an electric field acting on charged particles. The work done by an electric field E on a particle of mass m and charge e, during a time interval t, is

$$W = E\ e\ x = (E\ e\ t)^2\ /\ 2\ m \qquad (2.17)$$

As the mass of an electron is much smaller than the ion mass, energy will be transferred primarily to the electrons. Electron-ion and electron-atom collisions are not very effective in energy transfer, as has been mentioned earlier. In turn, the neutral atoms and ions share their energy efficiently in the collision processes and likewise lose energy to the walls of the chamber. The net result is that electrons can have a high average kinetic energy, which might typically be 2 to 8 eV. The ions have an energy not much higher than that of the neutral atoms, which gain energy above the ambient only by collisions with ions (effectively) and electrons (ineffectively) and remain essentially unchanged at room temperature.

Assuming a Maxwell-Boltzmann distribution of energies for neutral atoms and ions, the energy and temperature are related by

$$(1/2)\ M\ \overline{v^2} = (3/2)\ kT \tag{2.18}$$

$$\overline{v^2} = (3\ k\ T\ /\ M) \tag{2.18a}$$

where M is the mass of the atom or ion, $\overline{v^2}$ is the mean square of the speed, k is the Boltzmann constant, and T is the absolute temperature. As a first order approximation, we can also assume a Maxwell-Boltzmann distribution for the electrons in the plasma. This could be expected if the number of electron-electron collisions is large, and the energy sharing amongst the electrons is very efficient. An effective electron temperature is associated to the electron energy given by the above expression. Considering an average electron energy of 2 eV for a typical glow discharge, the corresponding temperature would be 23200 °K.

Since ions are able to get some energy from the electric field, their temperature is somewhat above ambient, a representative value being about 500 °K. The average velocity $\overline{v}$ can be evaluated from the expression

$$\overline{v} = (8\ kT/\ \pi\ m)^{1/2} \tag{2.19}$$

The electron density and positive ion density are equal on the average, and are refered to as plasma density.

When a substrate is suspended in the plasma, it is struck by electrons and ions with current densities proportional to their average velocities. As $\bar{v}_e >> \bar{v}_i$, therefore $j_e >> j_i$, and the substrate will tend to be charged negatively with respect to the plasma. As the negative potential builds up, the electron current density will decrease, but the substrate will continue being charged till it reaches a negative potential large enough so that the electron current density balances the ion current density. There will be a potential barrier in front of the substrate with the potential equal to the difference between the floating potential of the substrate V_s and the plasma potential V_p. Since electrons are repelled by this potential barrier, a positive space charge will develop around the substrate, forming a "sheath" with a lower electron density. As the glow of the discharge due to the relaxation of atoms excited by electron impact depends on the electron density and the energy of the exciting electrons, the substrate will be surrounded by a comparatively "dark space", a feature common to the sheaths formed around all objects in contact with the plasma. The potential barrier limits the number of electrons that enters the sheath from the plasma, but it also accelerate the ions that enter the sheath. In practice, the potential of the sheath above an electrically isolated substrate

varies from one or two volts upwards. The resulting kinetic energies must be compared with the interatomic binding energies in the thin film or substrate, which is typically of the order of 1 to 10 eV. Thus, it is reasonable to believe that a growing film on an electrically isolated surface in the plasma might be much affected by such impacts.

Debye length and Debye shielding. As the electron density and the ion density are nearly equal, their net coulomb interaction with a particular charge is zero. But, if some disturbance is introduced, say an additional charge Q, the instantaneous potential at that point is both non-zero and time dependent. The potential variation around the perturbation can be expressed by

$$V(x) = V_o \exp(-x/\lambda_D) \tag{2.20}$$

where $V_o = Q/4\pi\varepsilon_o r$ (2.21)

and $\lambda_D = (kT_e \varepsilon_o / n_e e^2)^{1/2}$ (2.22)

The quantity λ_D is known as the Debye length. The spatial dependence of V(x) indicates that if the potential in the plasma is perturbed, then the plasma reacts to oppose that change. The Debye length measures how rapidly the potential perturbation is attenuated in the plasma. For example, the Debye length is 105 microns for an argon plasma having an

electron density of 10^{10} per cubic centimeter and an electron temperature of 23,200 °K (corresponding to an energy of 2 eV).

Considering the effects of long-range forces in the collision theory, it can be shown that the force of interaction would be cut off at the Debye length. If an external voltage is imposed on a conducting element in the plasma, the electron and the ions around the object would react forming a sheath around it, leaving the plasma itself equipotential. Since the plasma is equipotential, then it is also electric field free, so that none of the constituent charged particles is subject to any externally imposed field, except to the extent that the plasma will respond to any further applied voltages by forming a screening sheath around the relevant electrode. Therefore, the charge assembly exhibits a collective behaviour, a necessary criterion for its classification as a plasma. A plasma is defined as a neutral collection of electrons and ions in which the Debye length is smaller than any boundaries surrounding the plasma.

If a plasma is perturbed from neutrality by any means, then there will be a large restoring force tending to re-establish charge neutrality. This restoring force is proportional to the displacement, which is just the condition for oscillation. The electrons, which are much lighter than the positive ions, will oscillate about their equilibrium position if the neutrality of charge is disturbed in any manner.

If we consider the positive ions to have fixed positions and the electrons to be displaced by a distance Δx, the angular frequency of their simple harmonic motion can be written as [15]

$$\omega_p = (n_e e^2 / m_e \varepsilon_o)^{1/2} \tag{2.23}$$

which corresponds to a plasma frequency of

$$f_p = 8{,}980 \; n_e^{1/2} \text{ Hz} \tag{2.24}$$

where n_e is the electron density in cm^{-3}. For a typical plasma density of 10^{10} cm^{-3}, the plasma frequency is 900 MHz. A period of this oscillation, which is about 1 nanosecond in this example, in fact gives the response time of the plasma to charge fluctuations.

The plasma frequency is related to the Debye length by

$$\lambda_D \omega_p = (\varepsilon_o k T_e / n e^2)^{1/2} (n e^2 / m_e \varepsilon_o)^{1/2} = (k T_e / m_e)^{1/2} \tag{2.25}$$

$$\lambda_D \omega_p \cong \bar{v}_e \tag{2.25a}$$

This means that the electrons can move a distance of about one Debye length in a time of $1/\omega_p$. If the plasma is disturbed by an electromagnetic wave of angular frequency ω, then the electrons can respond fast enough to mantain neu-

trality if $\omega < \omega_p$. Therefore, ω_p is the minimum frequency for propagation of longitudinal waves in the plasma.

From the wave propagation point of view we can write the expresion for the index of refraction of the plasma as

$$u = (1 - \omega_p^2 / \omega^2)^{1/2} \qquad (2.26)$$

When $\omega_p << \omega$, the index of refraction is near unity, and as the electron density increases the index of refraction approaches zero, and then becomes imaginary. A zero or pure imaginary index of refraction means that the wave can no longer propagate through the medium. Such a wave incident on a plasma boundary would therefore be reflected.

To study a plasma using electromagnetic techniques, it is necessary to operate in a regime where the wave can penetrate into (and also escape from) the plasma. For a typical microwave frequency of 9 GHz, the electron densities are limited to less than 10^{12} cm^{-3} .

From the plasma frequency relation we can define a <u>critical electron density</u> as

$$n_c = \omega^2 \, m \varepsilon_o / e^2 \qquad (2.27)$$

For densities below this critical value the plasma is nearly a transparent dielectric; and above it, the medium becomes opaque and highly reflecting. For a frequency of 2.45 GHz this critical density becomes 2.94×10^{12} cm^{-3} .

Diffusion. Whenever there is a concentration gradient of particles, the random motion of particles results in a net flow down the gradient. At very low charge concentrations, such as those encountered near breakdown, electrons and ions can be considered to diffuse independently of each other. The flux vector is given by

$$\vec{\Gamma} = - D \nabla n \tag{2.28}$$

where D is the diffusion coefficient of the particles of density n. Under steady state conditions, the charged particles lost from the ionized gas by diffusion must be replaced by ionization, and the continuity equation must be satisfied independently for both species.

$$D \nabla^2 n + n \nu_i = 0 \tag{2.29}$$

This equation has many solutions depending on the initial, and boundary conditions. The solution for a rectangular geometry of length L, width W, and height H is given by [17]

$$n_e = n_o \cos (\pi x/L) \cos (\pi y/W) \cos (\pi z/H) \tag{2.30}$$

where n_o is the electron density at the center of the box. Substitution of Eq. (2.30) to Eq. (2.29) leads to the constraint condition

$$\nu_i / D_e = 1/\Lambda^2 = (\pi/L)^2 + (\pi/W)^2 + (\pi/H)^2 \qquad (2.31)$$

where Λ is defined as the characteristic diffusion length, which is determined by the boundary conditions.

A similar treatment for a cylinder geometry of height H, with flat ends of radius R gives [17]

$$n_e = n_o \quad J_o \quad (2.405\ r\ /\ R)\ \cos\ (\pi z/H) \qquad (2.32)$$

in which J_o represents the zeroth order Bessel function. Again, by introducing Eq. (2.32) back to Eq. (3.29), we obtain the constraint condition

$$\nu_i / D_e = 1/\Lambda^2 = (2.405/R)^2 + (\pi/L)^2 \qquad (2.33)$$

The mobility and diffusion coefficient of the species obey the Einstein relation

$$D / \mu = k T_e / e \qquad (2.34)$$

The drift velocity per unit electric field (mobility) is inversely proportional to the mass of the particles. Under equilibrium conditions, the ion mobility is much smaller than the electron mobility, due to the big difference in mass of the two species. In turn, the ion diffusion coefficient will be much smaller than the electron diffusion coef-

ficient. Therefore, the process of free diffusion leads to a concentration of positive ions considerably higher than that of electrons. Under this condition the ionized gas can not be considered a plasma.

The separation of charge species caused by the difference in diffusion coefficients of electrons and ions produces a space charge field. The magnitude of this field will remain small, however, as long as the charge concentration remains low (e.g. $n < 10^2$ per cm^3) and, as a result, it will not affect the diffusion of either charge carriers.

As the charge concentration is increased, a level is finally reached at which the space charge field becomes sufficiently large to affect the transport of both electrons and positive ions. The ionized gas exhibits a collective behaviour and can properly be called a plasma. Then, electrons and ions will diffuse with the same diffusion coefficient: the ambipolar diffusion coefficient, D_a, which is given by

$$D_a = -(D_+\mu_e + D_e\mu_+)/(\mu_e + \mu_+) = D_+[1+(D_e\mu_+/D_+\mu_e)] \qquad (2.35)$$

$$D_a \cong D_+ \left(1 + T_e / T_g \right) \qquad (2.35a)$$

Ambipolar diffusion will usually occur when the electron and ion concentrations are approximately equal, and greater than about 10^8 per cm^3.

Transition Diffusion. When a discharge controlled by ambipolar diffusion is produced in a plane parallel plate geom-

etry, we would expect a sinusoidal electron spatial distribution, as can be seen from Eq. (2.30). However, in low power discharges, the ion density throughout the dicharge is not high enough to produce ambipolar diffusion throughout the volume, and then the discharge is ambipolar at the center, but controlled by free-diffusion coefficients at the walls.

Allis and Rose [2] have studied the transition from free to ambipolar diffusion theoretically, and compared their results with experiments in a microwave discharge set up in a resonant cavity. Their results show that the electron spatial distribution departs from the cosinusoidal distribution as expected for ambipolar diffusion, and then gradually becomes a bell-shaped distribution for a transition case as shown in Fig. 2.1 [7].

Diffusion of several species. When there is a mixture of electrons and positive ions, we would expect a single value of the ambipolar diffusion coefficient. However, if the plasma consist of electrons and two types of positive ions, there will be three different diffusion coefficients.

$$(D_a)_e \cong [(n_+)_1 / n_e]/(D_a)_1 + [(n_+)_2 / n_e] \quad (D_a)_2 \tag{2.36a}$$

$$(D_a)_1 \cong (D_+)_1 \quad (1 + T_e/T_g) \tag{2.36b}$$

$$(D_a)_2 \cong (D_+)_2 \quad (1 + T_e/T_g) \tag{2.36c}$$

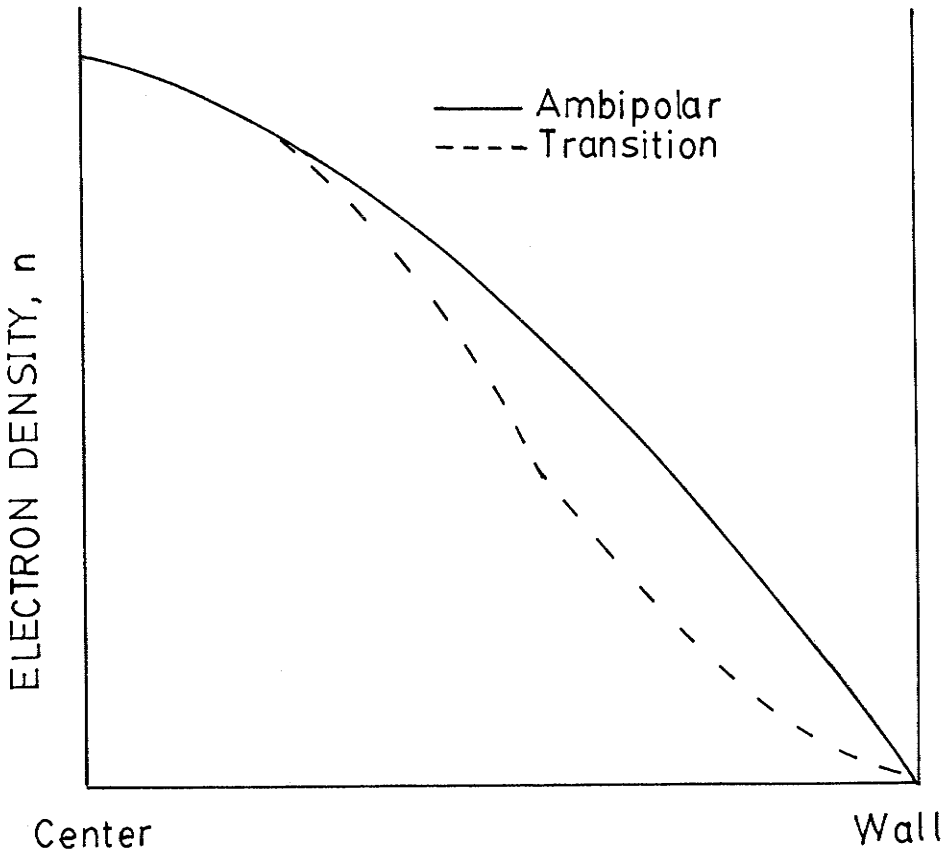

Figure 2.1: Electron spatial distribution between parallel plates.

This shows that although the diffusion of one ion is unaffected by the other, the electron diffusion coefficient can change depending on the relative concentration of each ionic species compared to the electron concentration[7].

Energy transfer The tranfer of energy to the plasma occurs principally through the action of the electric field on the electrons. In each collision with heavy particles, an electron's coherent motion is randomized. The heating effect, although small, is thus cumulative. From a calorimetric point of view electrons are heated by the electric field and cooled by collisions with heavy particles.

In a high frequency gas discharge, ionization caused by electron collision is responsible for causing the breakdown and for maintaining the discharge. The maximum kinetic energy for the oscillatory motion of an electron at the minimum experimentally determined field strength is of the order of 1 meV. It is therefore obvious that the energy of oscillation is insufficient to account for breakdown. In effect, electrons gain random energy on each collision until they are able to make an inelastic collision with a gas atom, thus leading to ionization. If an electron makes an elastic collision at an appropiate time with respect to the phase of the electric field, then its velocity and energy would continue to increase. In this way, electrons could reach ionizing energies at very low electric fields. This mechanism seems to be accepted as the dominant ionization source in

microwave discharges [28]. At such frequencies, the amplitude of electron motion becomes very small even for large fields. In addition, a large applied field can exist for a longer period before the plasma screens it out.

The power dissipated per unit volume in the electron gas by the electromagnetic wave is given by

$$P = 1/2 \; (\sigma_r E_o^2) \tag{2.37}$$

where σ_r is the real part of the conductivity and E is the peak amplitude of the electric field.

The Lorentz conductivity is given by [15]

$$\overset{*}{\sigma} = \sigma_r + j\sigma_i = ne^2 /m(\nu_c + j\omega) = \tag{2.38a}$$

$$= (ne^2/m)[\nu_c /(\omega^2+\nu_c^2)] - j(ne^2 /m)[\omega /(\omega^2+\nu_c^2)] \tag{2.38b}$$

Taking the real part of the conductivity, we obtain

$$P = (ne^2E_o^2 / 2m \; \nu_c)[\nu_c^2/(\nu_c^2+\omega^2)] \tag{2.39a}$$

When $\omega >> \nu_c$ Eq. (2.39a) reduces to

$$P = n \; e^2E_o^2 \; \nu_c / \; 2m \; \omega^2 \tag{2.39b}$$

The energy absorbed by the electron is proportional to the square of the electric field, and thus independent of its

sign. This indicates that the average electron can continue gaining energy in the field, despite the fact that it may be moving either with or against the field.

2.2 FABRICATION OF AMORPHOUS SILICON FILMS.

Amorphous solids lack long range periodic ordering in their lattice networks, but they have band gaps, analogous to those for single crystal semiconductors, indicating that short-range order remains in the amorphous network.

Amorphous silicon films are tetrahedrally coordinated and exhibit semiconductive properties. The chemical bonding structure of a tetrahedrally bonded network does not allow for flexibility. Therefore, an amorphous silicon network involves dangling bonds or defect states. The electronic activities of these unpaired localized states yield mid-gap states in a material with a relatively small density of diffused band edge states. But, the density of states (DOS) in the gap is very much dependent on the fabrication technique. Techniques that allow hydrogen incorporation into the a-Si films have yielded a-Si:H films sensitive to doping, suitable for solar cell fabrication. Methods for preparation of a-Si and a-Si:H films will be briefly reviewed, along with their most relevant properties.

2.2.1 Thermal evaporation.

Solid material heated to a sufficiently high temperature vaporizes. The vapors may be condensed onto substrates. To ensure no contamination from ambient gas atoms, silicon is evaporated under ultra high vacuum conditions, 10^{-10} torr or better. A large distance between the source and the substrate is generally used to achieve good thickness uniformity. The ultra clean and smooth substrate is usually maintained at 250 to 300 °C during deposition. For high melting point materials, such as silicon, heating by electron bombardment is used. Very high temperatures are attainable by this method. Since only the material close to the surface is heated, this method can also avoid contamination.

Vacuum evaporated a-Si films have a high DOS in the gap. Their optical and electrical properties are very much affected by the ultimate vacuum of the ultra-high vacuum system and by the deposition rate. These properties have been correlated with oxygen incorporation into the films [4,5].

2.2.2 Sputtering

The sputtering process, in which atoms are ejected from the surface of a material by high energy ionic bombardment, can be used for the deposition of a-Si films. A glow discharge is a convenient method of producing a significant flux of gas ions. The "target" material subjected to ionic bombardment is normally a prefabricated polycrystalline wafer, or

compressed powder. The ion impact may set up a series of collisions between atoms of the target, possibly leading to the ejection of some of these atoms, which, under the right circumstances, move through space until they strike and condense on the substrate. Argon, or other inert gas, is used as the sputtering gas in order to avoid chemical reactions with the target or the growing film. Argon atoms have been found entrapped in sputtered silicon films up to a concentration of one atomic percent [35]. The argon content in the film decreases with gas pressure. This suggests that neutral atoms and ions lose energy in gas phase collisions, which reduces the chance for shallow Ar implantation [35].

Amorphous silicon films prepared by sputtering in argon always appear to have a high DOS in the gap, in particular at the energy of the Fermi level. The deliberate incorporation of hydrogen into a-Si during its production by sputtering has been shown to lead to dramatic differences in properties from those of unhydrogenated silicon. For example, the spin density and the electrical conductivity are both decreased by several orders of magnitude and the absorption edge is shifted to higher energy by several tenths of an eV [35,10,11]. Films are usually prepared in a rf glow discharge of a gas mixture of argon and hydrogen. Unhydrogenated a-Si films prepared by sputtering techniques have similar properties to those prepared by thermal vacuum evaporation.

For a full review on the different sputtering techniques for thin film deposition, the reader is refered to the book of J.L. Vossen and J.J. Cuomo[44].

2.2.3 Chemical Vapor Deposition (CVD).

Chemical vapor deposition has been used extensively for the growth of epitaxial layers of silicon and germanium from the thermal decomposition (pyrolysis) of the parent gases, silane (SiH_4) and germane (GeH_4). In CVD, the volatile compound of the substance to be deposited is vaporized, and the vapor is thermally decomposed or reacted with other gases at the substrate to yield non volatile reaction products which deposit atom by atom on the substrate. An excellent review on CVD has been published by W. Kern and V.S. Ban in reference [44].

Silane is a colorless gas which ignites spontaneously when released into the atmosphere. Its boiling point is 161 °K and its melting point is 88 °K. The mixture of silane and air is explosive over a wide range of compositions. Silane has a positive free heat of formation which is about +7.5 kilocalories per mole. The pyrolytic reaction

$$SiH_4 \quad ----> \quad Si \quad + \quad 2\ H_2 \qquad (2.40)$$

is appreciable at temperatures above 600 °C and is accompanied by the formation of small amounts of polymers, such as

disilane ($Si_2 H_6$), trisilane ($Si_3 H_8$), etc. The standard free energy of decomposition for this reaction is -12 Kcal per mole at 300 °K and -40 kcal per mole at 1400 °K.

Doped a-Si films have been grown by thermally decomposing a silane-phosphine mixture at 650 °C for the n-type or silane-diborane mixture at 550 °C for the p-type a-Si:H films [42,16]. Hirose et al. [16] have reported that phosphorous doping of CVD a-Si films can remove a significant portion of gap states as well as most of the electron spin resonance ESR centers, and that hydrogen ion implantation remarkably enhances doping efficiency and drastically increases photoconductivity.

2.2.4 Plasma enhanced chemical vapor deposition, PECVD. Electrons in the glow discharge possess sufficient energy to break molecular bonds. Thus, chemical reactions can occur at a relatively low temperature, typical deposition temperatures being 200 to 300 °C. Conventional CVD requires a much higher temperature, which may be inappropriate for certain substrate materials or device structures. The films that are deposited by plasma reactions are usually amorphous in nature.

Amorphous silicon films deposited by glow discharge decomposition of silane gas is highly hydrogenated, and they are in fact silicon-hydrogen alloy films. Their properties depart drastically from the unhydrogenated film deposited by

the methods previously described. The importance of a-Si:H films was not fully realized until Spear and Le Comber succeded in doping them in 1975 [39]. Amorphous silicon films produced by this deposition method have several remarkable properties, such as large photoconductivity and excess carrier lifetime, efficient photo and electroluminescence, and low concentration of unpaired spins (dangling or unsaturated bonds). These desirable properties are not so much due to the absence of structural defects, but due to the high concentration of hydrogen atoms, which is of the order of 10^{22} cm^{-3} (between 10 and 35 atomic percent). This is about a hundred times larger than the maximum number of dangling bonds which has been observed in unhydrogenated a-Si. The hydrogen is therefore not just playing a role in saturating dangling bonds, but also in modifying the whole structure, so that the material becomes indeed, a silicon-hydrogen alloy. Films with similar optical and electrical characteristics can be prepared equally well by radio frequency sputtering in the presence of hydrogen [35,34].

In the glow discharge there are many species with more than enough energy to rupture any chemical bond. Complete bond scrambling can occur, and often bonding is found in the deposit which exists nowhere in any reactant. The storm of energetic electrons and ions tears the reactants apart [17,31]. Since most of the resulting fragments are themselves reactive, their reassembly to form a product film

will be almost random. This aspect of PECVD makes close control of all variables imperative for reproducible results, but it has its advantages too. It is possible to adjust the composition, and the physical or electrical properties of a film over a considerable range, much more readily than with other deposition methods.

Once chemically reactive species have been generated in the discharge, a wide variety of reactions can occur. Homogeneous reactions which influence the composition of the discharge may be as follows.

Ionization

$$SiH_4 + e \longrightarrow SiH_4^+ + 2\,e \qquad (2.41)$$

as well as ionization of radicals SiH, SiH_2, SiH_3, and of H_2. These reactions are important to sustain the discharge.

Electron attachment.

$$SiH_4 + e \longrightarrow SiH_4^- \qquad (2.42)$$

as well as the electron attachment to radicals. These reactions represent one of the means by which the discharge loses electrons, the main one being collisions with the walls and electrodes.

Dissociation. These are the most important reactions for the properties of the deposited films, since they are re-

sponsible for the hydrogen generation. The most frequent dissociation reactions are [25]:

$$SiH_4 + e\ (> 3.5\ eV) \longrightarrow SiH_3 + H + e \qquad (2.43)$$

$$SiH_4 + e\ (> 6.9\ eV) \longrightarrow SiH_2 + 2H + e \qquad (2.44)$$

$$SiH_4 + e\ (>10.4\ eV) \longrightarrow SiH + 3H + e \qquad (2.45)$$

$$SiH_4 + e\ (>14\ eV) \longrightarrow Si + 4H + e \qquad (2.46)$$

The radicals SiH_3, SiH_2, and SiH are unstable and may be decomposed by collisions with electrons.

Heterogeneous reactions occur at the substrate surface and at the walls. Some of them are given as follows:

$$SiH_4(gas) \xrightarrow{surface} Si\ (sol.) + 2\ H_2(gas) \qquad (2.47)$$

$$SiH_3(gas) \xrightarrow{surface} Si\ (sol.) + 3/2\ H_2(gas) \qquad (2.48)$$

etc., but also

$$SiH_3(gas) \xrightarrow{surface} SiH_3\ (solid) \qquad (2.49)$$

$$SiH_3(gas) \xrightarrow{surface} SiH_2\ (solid) + H\ (gas) \qquad (2.50)$$

etc.

The rate constants of these reactions depend on the properties of the colliding species and the nature of the substrate and its temperature [22]. According to Knights [22] the growth model for the a-Si:H film may be as follows. Substrate dependent nucleation is followed by the growth of islands until the island boudaries are in close proximity. Depending on the surface chemical reactions and energy mini-

mization, two extreme situations may arise. In the first an $(SiH_2)_n$ polymer phase forms, which provides an elastic bond over at least part of the interfaces. Defects are probably located on or near these interfaces and residual stress in the structure is minimal. The second situation can be visualized initially in the absence of hydrogen as being the coalescence of a series of continuous random network structures of diameter approximately 100 Angstroms. This would on the average create partly bridged interfaces with a large number of dangling and strained bonds. Hydogenation of these interfaces would result in the removal of the dangling bonds and probably the scission of some of the more strained bonds, but would still leave some stress in the structure and an inhomogeneous distribution of both defects and hydrogen. The model of Barna et al. [6] assumes nucleation and growth via the capture of mobile species that tend to satisfy the maximum number of dangling bonds. Knights [22], using Barnas'model, has concluded that a major difference between evaporation and glow discharge deposition is the enhanced surface mobility in the latter. Knights has proposed that the diffusing species are SiH_3 and SiH_2, and that because they have one or two dangling bonds, their strength of attachment to a surface site would be low and the mobility high. Furthermore, plasma deposition permits island coalescence to be almost perfect under certain conditions.

2.3 THE PECVD SYSTEMS.

Because of the largely empirical operation and control of plasma processing, it is worthy to give a brief account of the equipment and deposition parameters involved in the PECVD systems. Present commercial-scale equipment, such as those used in silicon integrated circuit processing, is almost always of the Reinberg radial-flow type, with a deposition chamber as shown schematically in Fig. 2.2. Typical diameter of the deposition chamber is about 60 cm, and the interelectrode distance is about 5 to 7 cm. This size of the chamber can handle up to twenty five wafers of 3 inches in diameter. Tube reactors have not satisfied the film thickness uniformity requirements. Deposition rates are commonly in the range of 2 to 80 Angstroms per minute. The total gas flow, which depends on the size of the system and the film deposited, is in the range of 5 to 100 sccm. The gas pressure is limited at the lower end by the mean free path ; it should not be so low that collisions could become too infrequent, and this sets the lower end at about 0.1 torr. On the other hand, if the pressure is higher than about 5 torr, filamentary discharge and other plasma instabilities may appear. This would promote homogeneous nucleation since decomposition then occurs predominantly inside the plasma, rather than at the substrate surface [13]. Residence time in the plasma is only about one second. Deposition efficiency is low, as it is with most glow discharge chemical vapor depo-

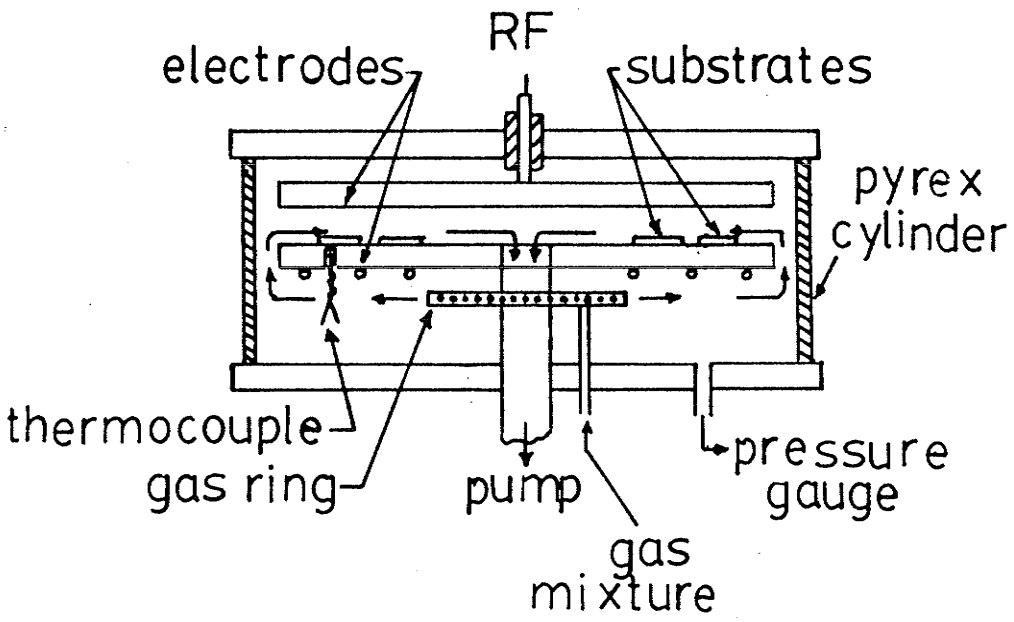

Figure 2.2: Reindberg radial-flow type reactor.

sition reactions. Less than 20% of the reactant species may end up as deposited films; the remainder produces a collection of disposal and maintenance problems.

2.3.1 Standard requirement for PECVD systems.

The main components of a PECVD system are the deposition chamber, the energy source for the plasma, gas network, vacuum system, and the safety valves, shieldings, and interlocks. The requirement for each component, and for the system as a whole, depend on the main use, but they are also dictated by experience in making the equipment as safe and reliable as possible for its operators. For experimental equipment, many of the requirements can be relaxed, relying on the knowledge and the patience of the operators.

Deposition chamber. Deposition chambers should be built with high quality materials, such as stainless steel and quartz, in order to withstand baking at high temperature. Vacuum seals should be made of copper if they are to be baked to 400 °C, or viton O-rings when not exposed to high temperature or to the plasma. The deposition chamber should be provided with a substrate holder (or table) that could accomodate a heater so that the substrates could be heated to 350 °C or more. A shutter should be provided to mask the substrates or the film against unwanted impurities arising from initial instabilities of the discharge, and to ensure reliable and constant deposition conditions throughout the

fabrication period. An electrical feedthrough is needed for heater, thermocouples, plasma probes, and plasma trigger electrode connections. Windows for visual observation of the plasma are a necessity, but they are also desirable for OES, optical absorption spectroscopy OAS, and for microwave plasma diagnosis (reflection, transmission, scattering, etc.). Quartz windows should be used to allow for ultraviolet OES. Other requirements for the chamber should be:

1. Electrodes accurately parallel and flat, with adjustable spacing.
2. High and low vacuum gauges.
3. Isolation transformer for resistance heaters.
4. Ready access to all parts of the chamber for cleaning.
5. Provision for fast and symmetrically uniform dispersal of gas stream.

Gas stream preparation. Gas mixtures should be prepared in a totally enclosed and ventilated area if hazardous gases are to be used. The plumbing should be designed to permit leak isolation and location, with provisions for purging gas lines back to the tank valve. Automatic flow control via mass flowmeters for a flow range 0 to 1000 ccpm are desirable. Gas line submicron filters and purification facilities for each gas line are needed for critical applications where impurities are a concern.

Vacuum systems. Deposition processes impose harsh requirements on vacuum pumping system because of the corrosive nature of the gases employed. Depending on the desired film, the gases may be SiH_4, NH_3, PH_3, AsH_3, N_2, and O_2, or mixtures of these. The products of decomposition may include H_2, O_2, H, and O. The vacuum system is also required to handle colloidal SiO_2, Si_3N_4 and silicate particles, which can be in the effluent going to the pump. It is evident that the effluent leaving the reactor and entering the vacuum system may be corrosive, flammable, explosive, toxic, or may tend to form gummy deposits in the pump. Vacuum pumps should be able to pump up to 300 cfm or more, depending on the size of the reactor and the operating pressure.

A diffusion pump should be incorporated in the system to reach an ultimate vacuum of 10^{-6} torr or better, prior to deposition. A mechanical pump of the rotary piston type can withstand the effect of particulate matter and chemical corrosion without excessive maintenance and curtailed pump life. A mechanical pump equipped with a roots blower extends the vacuum operation range to 10^{-3} torr and reduces oil vapor backstreaming from the rotary pump into the discharge. Other desirable features are:

1. Vibration-isolation from deposition chamber.
2. Large, cleanable particulate trap upstream of the pumps.

3. Chemically inert oil, such as Fomblin or Halocarbon, for the pumps.
4. Exhaust with purging capability and failure alarm.
5. Ready access to the pumps for frequent pump oil changes.
6. Closed loop chamber pressure control via motor driven throttle valve.

Energy source for plasma. Power supplies for glow discharges can be of many different types. Most of the PECVD systems are driven by rf power at a frequency of 13.5 MHz, but there are reports about systems operating at frequencies from dc, 10 kHz [12], to microwave range [32]. The power level is small, typically 10-20 W. Deposition rate does appear to be affected by the pulsing of the high frequency power [14,45].

Safety considerations. A number of safety procedures in dealing with plasma systems must be enforced strictly. Gases that are contained in cylinders should be treated with the utmost respect. Working with compressed gases, we need to be specially aware of the physical state of the material inside the cylinders, the chemical hazards of the material, the physical hazards of the cylinder itself, and the proper safety precautions pertaining to the use of the material and its cylinder. The physical characteristics of a gas or liquid may constrain the design of the physical system. The reaction products of a plasma process may determine requirements for cold traps, the type and number of pumps used, the

level of gas monitor sophistication, or the use of endpoint detection. The flammability of a material will determine whether the gas cabinet in which the cylinder is placed requires positive pressure of an agent other than air to flush the exhaust; or whether a burn-box should be used on the exhaust side of the reactor to avoid the possibility of gas accumulation and possible explosion. Cylinders containing flammable materials should be electrically grounded to avoid static charge accumulation. But, the most important single safety factor is the awareness of the workers of every possibility of risk, along with an understanding of the physical and chemical processes going on in the different sections of the system.

2.3.2 Microwave hardware.

The main type of generators capable of producing power suitable for plasma chemical work are magnetrons, klystrons, backward wave oscillators (BWO), and travelling wave tubes (TWT).

Magnetrons are diodes in which a magnetic field is applied at right angles to the electric field between the cathode and the anode. The tuned circuit included in the tube takes the form of cylindrical cavities opening into the central portion via narrow slits. The magnetron is a fixed frequency generator with a power range from about 100 W to over 3kW at 2.45 GHz. They are simple to operate, rugged, have

good efficiency, and are relatively low priced. The upper frequency range of magnetrons and klystrons extends to above 50 GHz. However, the physical size of waveguide and resonant cavities imposes practical limits to the frequency that can be used for discharge work, and this limit probably is at about 10 GHz.

Many magnetrons and klystrons are designed for pulsed operation in radar units. Typical pulse widths are 0.01-5.0 microseconds, and repetition rates are from 200-10000 per second. Because power is dissipated only during the pulse, it is possible to obtain very high pulse output from relatively small tubes. Typical peak power outputs range from several kilowatts for small tubes to many megawatts. Not a great deal of research has been done on the effects of pulse power in discharges. Shaw [37] has reported no significant difference between cw and pulse power in the producion of atomic hydrogen at frequencies of 3 and 9 GHz, with average powers of 5-300 W. Yasuda [45] has reported that for organic compounds plasma polymerization the pulsing of the high frequency power does have an effect on deposition rates: the polymerization rate could be either increased or decreased by as much as 100%, depending on the structure of the starting compound. Pulsed rf discharge has been used for studying the growth kinetics of a-Si:H films by Hamasaki et al. [14]. They have found that the growth rate of a-Si:H and the hydrogen content of the films do not depend on the repetition

frequency of the modulated rf excitation, but the deposition rate is increased with the duty cycle, while the hydrogen content remains unchanged. They interpreted their results as due to the fact that the gas phase polymerization is not predominant in the silane plasma, and that the growth takes place through the heterogeneous reactions of adsorbed chemical species on the substrate surface.

BWOs can be tuned over the range 2:1 and are capable of delivering several kilowatts of power. TWTs are primarily amplifiers of rather limited power. While the last two generators may be worthy of consideration, magnetrons represent the best choice on the basis of cost and simplicity of power requirements.

Power adjustment. It is a characteristic of magnetrons that a certain high voltage must be applied to the anode before oscillation starts. Thereafter, a maximum power is reached at a voltage which may be 10-15% higher than the starting value. Power to the load may also be controlled by inserting a variable attenuator between the generator and the discharge tube, but at power higher than 200 W, a wasteful amount of energy must be dissipated.

Waveguide and waveguide resonators. Waveguides, which are metal tubes usually of rectangular or circular cross section, are employed to transfer microwave energy. Since there is no radiation, and very little dielectric loss, attenuation of the power transmitted is very small. The rectangular

section waveguide is the one most commonly employed. Below a certain frequency, known as the cut off frequency, a waveguide of a given size can not transfer energy. The cut off wavelength, λ_c, is given by $\lambda_c = 2$ b, where b is the larger dimension in a rectangular waveguide of dimensions a and b. In most waveguides, however, b instead of being made equal to $\lambda_c/2$, is $0.7\,\lambda_c$, to allow for small variations in frequency. The b dimension for a 500 MHz guide should be approximatelly 17.5 inches (44.45 cm), which is physically rather large, and that for a 10 GHz guide is about 1 inch, which is as small as can be conveniently used for discharge work.

It is possible for a guide to transmit energy of frequencies higher than its cut-off frequency; including frequencies that are multiples of the latter by means of more complex modes than the fundamental, but a discussion of these other modes is beyond the scope of the present chapter.

If a short circuit is introduced into the waveguide at a position that causes virtually total reflection of the energy travelling down the waveguide, standing waves will be set up. A very satisfactory resonant cavity can be formed in this way, and since there is no loss due to radiation, this simple resonant cavity is well suited to the production of plasmas in gases. It may be used for this purpose by inserting a quartz tube carrying the gas at a point of maximum

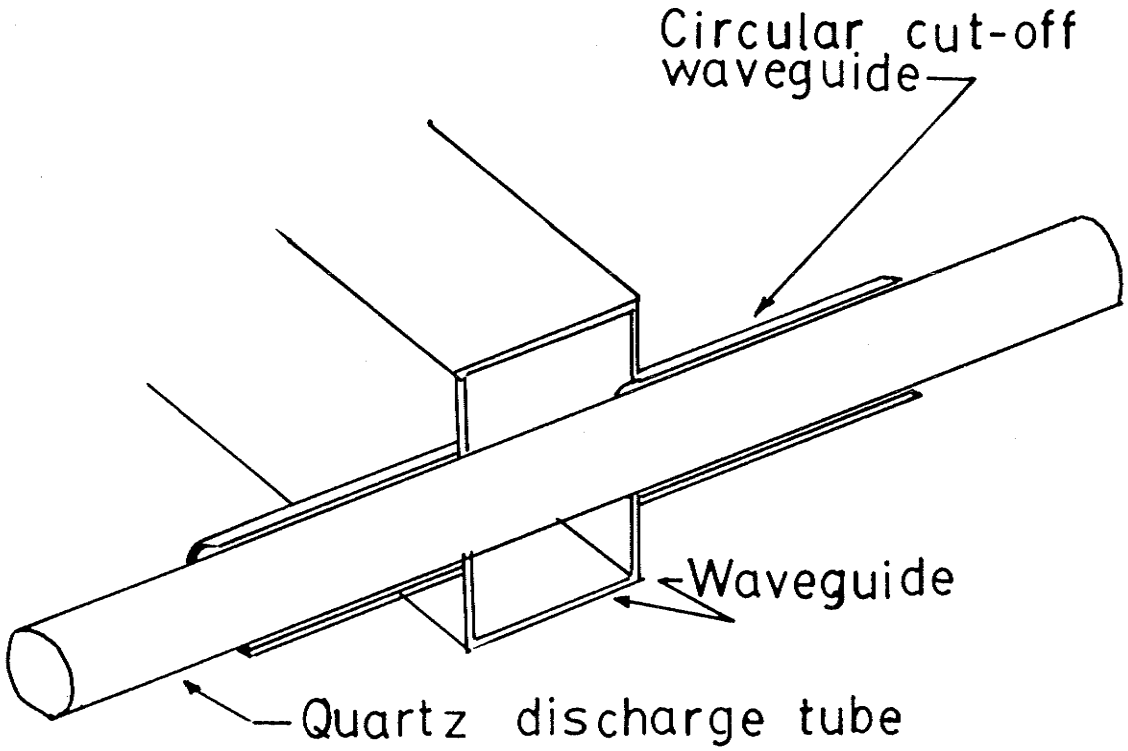

Figure 2.3: Discharge tube in a waveguide.

electric field. The tube should be of quartz or Vycor, both of which have low dielectric loss at microwave frequencies and hence do not absorb apreciable power; they also have high melting points.

When the discharge tube is placed transversally through the waveguide, as shown in Fig. 2.3, the electric field, which is responsible for accelerating the electrons in the plasma, is oriented parallel to its axis. Hence the most energetic electrons will tend to be those moving in the direction parallel to the walls of the tube, and thus sputtering of the tube is reduced if not eliminated. In Fig. 2.3 the short cylindrical metal tubes enclosing the discharge tube on either side of the waveguide serve to prevent propagation of the microwave energy along the tube, thus restricting the field to the interior of the guide.

At powers above 200-300 W, water-cooling of the guide and guard tubes may be desirable. For this purpose small diameter copper tubing is brazed onto the walls. Forced-draught cooling of the region of the reaction tube that is within the guide may also be required, which may be effected by blowing air through the guide itself via small holes in the metal walls, which neither radiate nor seriously affect the tuning.

One of the simplest forms of waveguide resonator is shown in Fig. 2.4. The microwave energy is fed in approximately one quarter wavelength from the closed end at a point

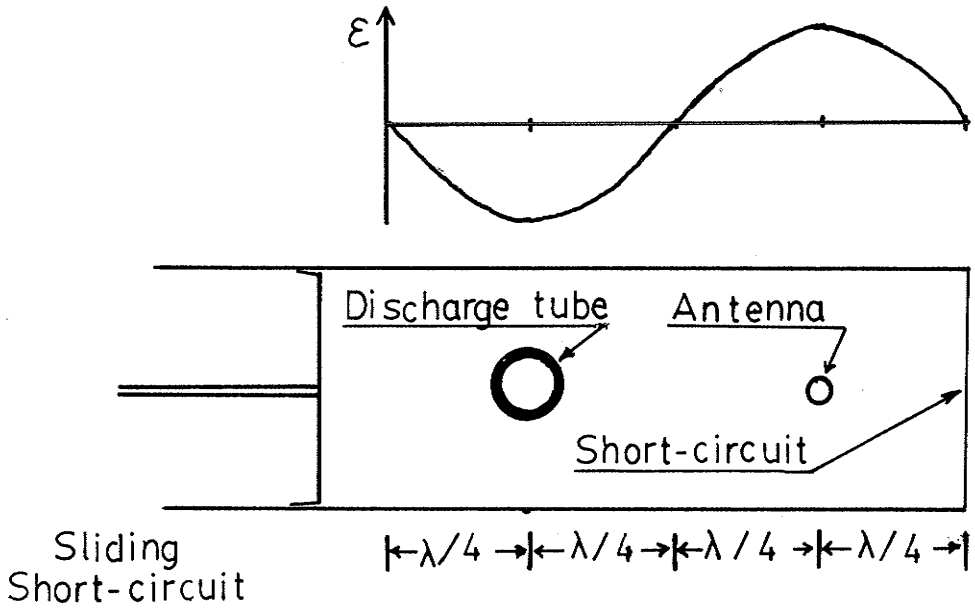

Figure 2.4: Waveguide resonator.

which becomes a voltage antinode. One half wavelength further along the waveguide, openings are made to accommodate the discharge tube, and the adjustable short crcuit is placed approximately one quarter wavelength beyond this point.

Protection of generators. Short circuits are deliberately introduced in microwave plasma chemistry systems to reflect incident energy and to set up standing waves. Thus, considerable reflected power could reach the magnetron unless some sort of protection is introduced in the microwave system. Devices such as isolators and circulators are frequently used. Isolators are somewhat limited in their power handling capabilities; while circulators, since they do not dissipate power, may have higher ratings and are more frequently used. Ideally, the load should absorb all the incident power, and in fact it absorbs the greater part of it when impedance matching is correct. But in plasma chemical applications matching seldom happens: if the discharge extinguishes, practically all the power may be reflected back into the generator.

Chapter III

MICROWAVE PLASMA CHEMICAL VAPOR DEPOSITION SYSTEMS.

The Materials and Devices Research Laboratory, at the University of Manitoba, had previously developed a microwave sputtering system that had succesfully sputtered selenium pellets and deposited amorphous selenium thin films [18]. Films were deposited on substrates placed in a deposition chamber distant from the plasma region to prevent substrate bombardment. Later, we converted this sputtering system to a microwave plasma chemical vapor deposition (MPCVD) system in order to deposit silicon films from the plasma decomposition of silane gas. Three different system configurations have been explored in the course of this work. The first two are basically the same, with the exception of the direction of flow of the gas stream. To distinguish between them, the first two systems are referred to as the "discharge tube-chamber" configuration I and the "discharge tube-chamber" configuration II, and the third one as the "short circuited waveguide chamber" configuration; the latter is an entirely different approach. In the following we shall describe the microwave generator, the vacuum system, the gas network, and the exhaust system that are common to all three configurations, and then compare and discuss our approach with other film deposition systems.

3.1 THE DISCHARGE TUBE-CHAMBER CONFIGURATION I.

3.1.1 The discharge tube, the power supply, and the chamber.

The microwave sputtering system, converted later to a plasma chemical vapor deposition system, is based on a coaxial line type discharge tube cavity as shown schematically in Fig. 3.1. It is basically a transition from a waveguide to a coaxial line. The outer conductor of the coaxial line is a metallic cylinder attached to the H-plane of the waveguide by a tapered section. A quartz discharge tube is inserted coaxially to the metal cylinder. When the plasma frequency is larger than the microwave excitation frequency the plasma plays the role of the center conductor of the coaxial line. Thus a cylindrical plasma uniform along the radius of the discharge tube can be produced [19].

The microwave power supply is guided by a rectangular waveguide WR-284 to the waveguide-coaxial line transition. The microwave power supply is based upon a magnetron: a Phillips YJ 1160 coaxial output, water-cooled tube, matched to a WR-284 waveguide. The average output power is 3 kW at a frequency of 2.45 GHz under a pulsed oscillation mode. Using a filtering circuit for the dc high voltage, continuous-wave microwave power up to 1000 W has been obtained. The ripple on the microwave power is lower than 5%. A circulator and dummy load, a directional coupler, and an E-H tuner are used to control the microwave excitation power, as shown in Fig. 3.1.

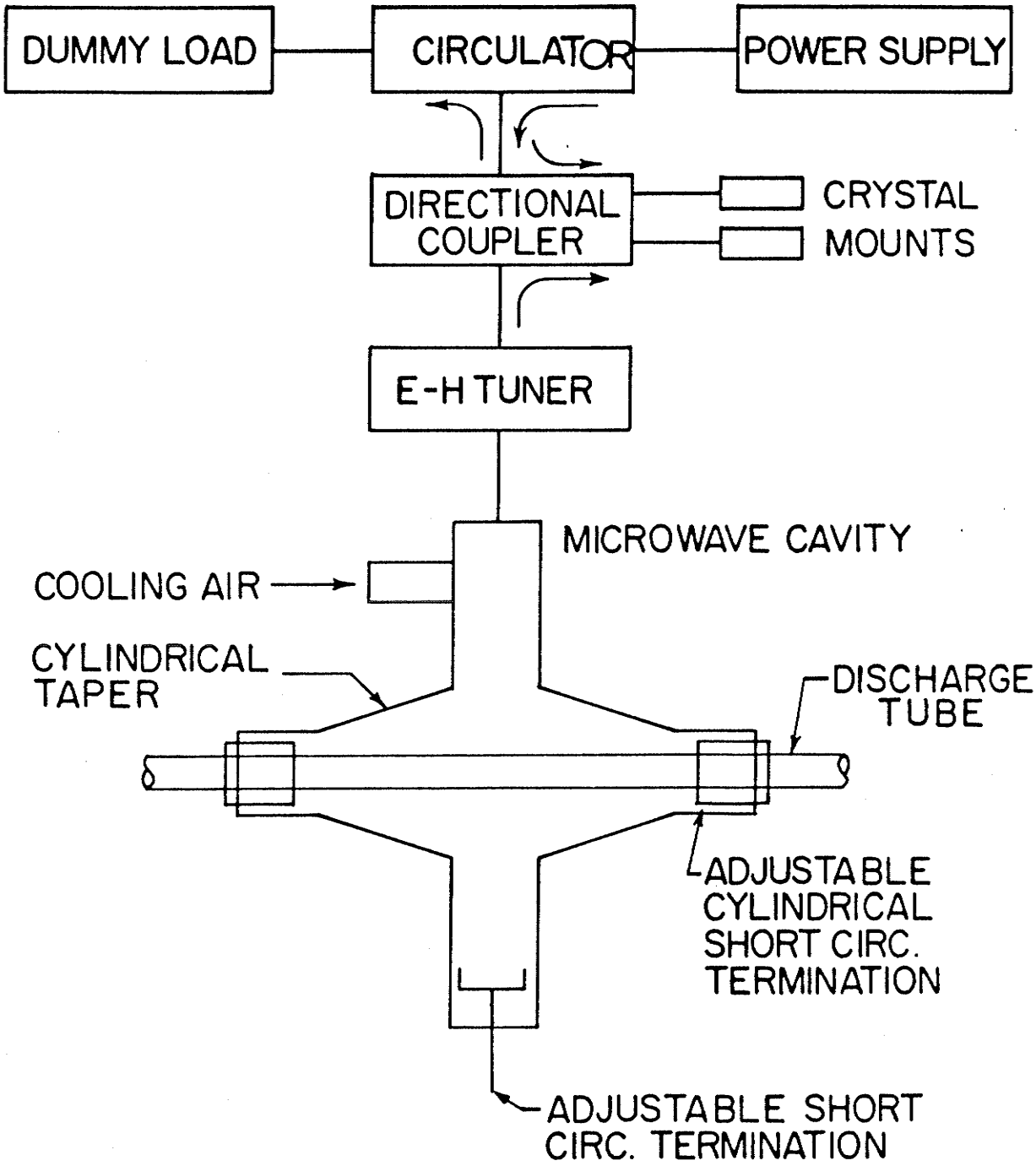

Microwave power circuit and configuration of the coaxial line microwave cw discharge tube.

Figure 3.1: Power generator and discharge tube.

One end of the discharge tube is coupled to the deposition chamber which is a glass cylinder with an adjustable substrate holder inside it, and the other end is connected to the pumping system, as shown in Fig. 3.2. An ultimate vacuum better than 10^{-6} torr can be attained in the chamber.

3.1.2 The gas network.

The gas network system was designed to meet the following requirements:

1. Silane, germane, hydrogen, and argon had to be safely handled.
2. Gas mixtures could be accurately prepared.
3. Pressures and flow could be reliable measured.
4. Contamination, due to background gases in the lines, could be reduced to an acceptable level.
5. Gases of commercial semiconductor grade could be further purified.
6. Unreacted gases or products of decomposition could be safely disposed of.
7. In spite of the safety requirements and the research requirements, the gas network could be affordable.

Some of the components used in the final design are shown in Fig. 3.3.

These stringent requirements imply that the system had to be leak proof and vacuum tight, with components capable

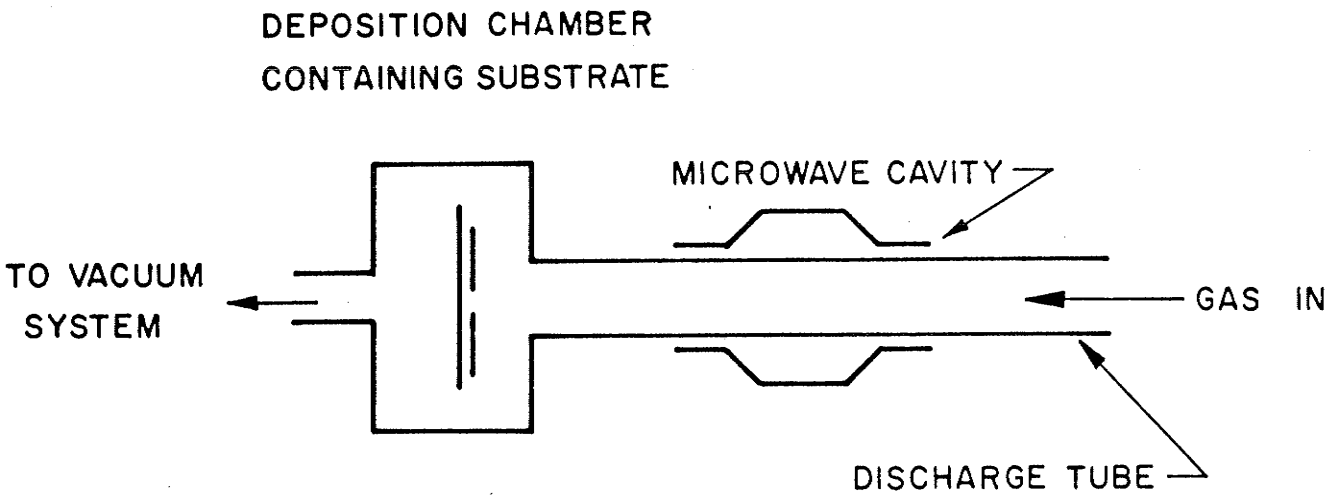

Figure 3.2: Discharge tube-chamber configuration I.

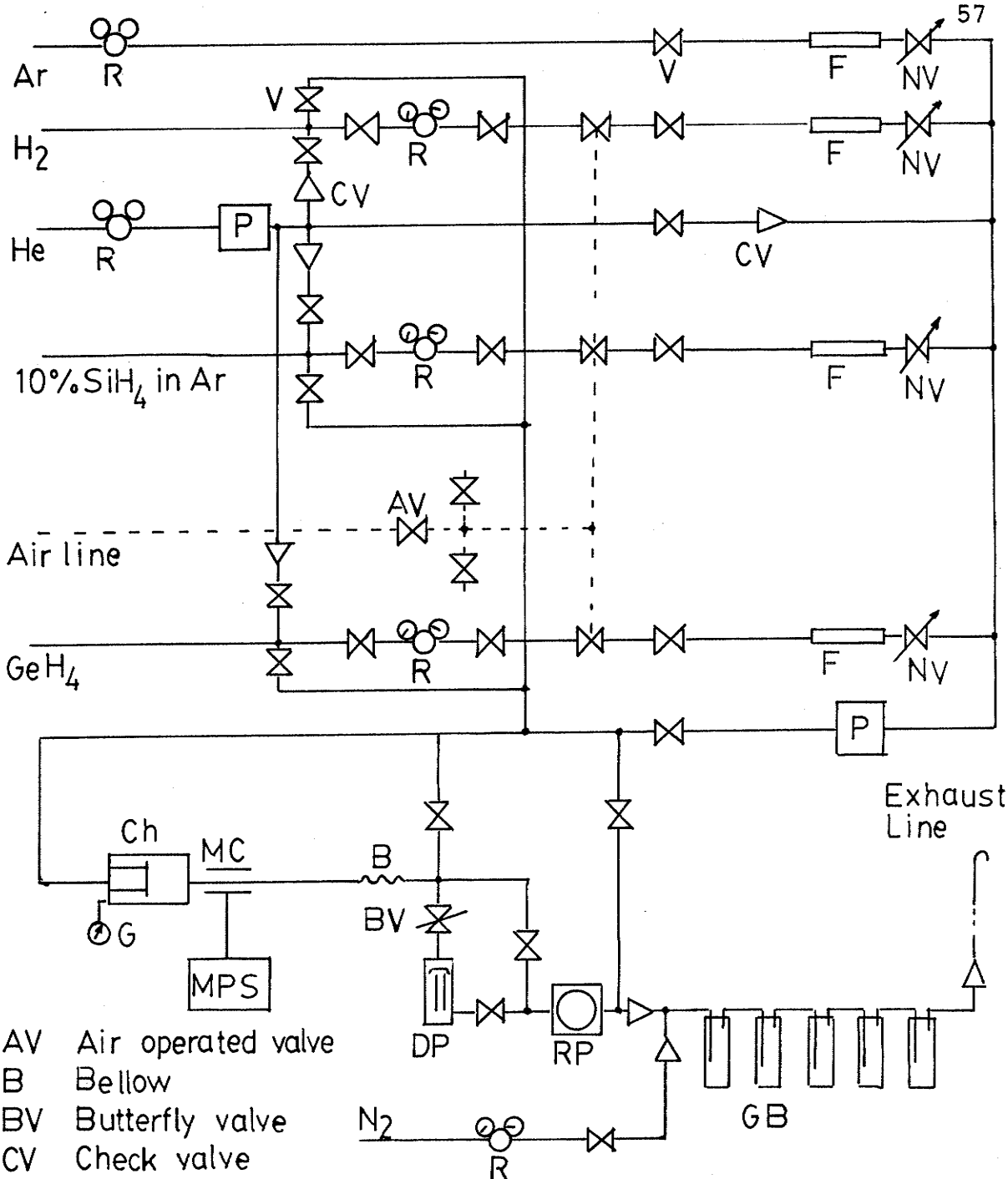

AV	Air operated valve	MPS	Microwave power source
B	Bellow	NV	Needle valve
BV	Butterfly valve	P	Gas purifiers
CV	Check valve	R	Gas regulator
DP	Diffusion pump	RP	Rotary pump
F	Flowmeter	V	Valve
Ch	Chamber		
G	Vacuum gauge		
GB	Gas washing bottle		
MC	Microwave cavity		

Figure 3.3: Gas network and exhausted system.

to withstand pressures as high as 6000 psig and vacuum of 10^{-6} torr. The toxicity and flammability of some gases such as silane and germane dictated the materials to be used in lines and components. Gas lines, fittings, valves, gauges and flowmeters were specified as 316 stainless steel construction, with teflon sittings for valves, and no pocket volumes in valves, regulators, gauges, or lines. Cross purge assemblies were used at the cylinder connections of all spontaneously flammable gases. Air operated valves, that could be turned off either from the experimental bench or from the access door to the laboratory were installed in each line supplying hazardous gases. Check valves were installed in order to avoid inadvertent flow of gases to inert gas lines, or feedback loops between exhausted gas lines and regions under vacuum. Gas line submicron filters and Hydrox purifiers were used to further purify commercial semiconductor purity gases. A dynamic gas mixture unit, capable of mixing silane, germane, argon, and hydrogen gases was used. Facilities for static gas mixture, with high accuracy pressure gauges were also incorporated into the system.

Exhaust gases were disposed of by scrubbing them through a caustic solution (10% sodium hydroxide) in five gas washing bottles, and then delivering any remaining gas, mainly hydrogen, through a 1/4 inch stainless steel tube all the way up to the roof of the building where they spontaneously ignited and burned in contact with the air. The ex-

hausted gases were previously diluted with nitrogen. Nitrogen was also used for purging the exhaust line, while the rest of the lines were purged with helium, which also served to check the lines for leaks by using a helium leak detector.

3.1.3 Experimental work.

The first series of experiments was conducted using configuration I of the microwave sputtering system as shown in Figs. 3.1 and 3.2. The gas mixture was admitted to the discharge tube in the microwave cavity and then into the deposition chamber. The configuration had previously been used as an sputtering system using argon or helium gases [18]. A stable argon gas discharge was obtained at a pressure of 0.1 torr, an incident power of 200 W, and a reflected power of 100 W. Substrates were placed on the substrate holder in the deposition chamber and maintained at room temperature. Instead of placing selenium pellets in the discharge tube, as the sputtering deposition required, a gas mixture of 10% silane in argon was fed to the discharge tube. With this gas mixture, it was quite difficult to trigger the discharge; and even when it could be triggered a higher level of power was required for maintaining the plasma. An initial stable discharge was obtained with 620 W incident power, 55 W reflected power, and 60 mtorr pressure. A silicon film started to deposit on the inner walls of the discharge tube,

mainly at the input of the cavity, and as the film grew thicker, the deposition moved toward the center of the cavity but no film was deposited on the substrates.

The microwave energy was very efficient in dissociating the silane gas, at least at that level of power. The dissociation occured as soon as the silane molecules met the plasma, and the dissociation products diffused a short distance, in both directions, along the discharge tube and condensed on its walls. The T-shaped discharge tube, the microwave cavity, and the deposition chamber are shown photographically in Fig. 3.4.

Since the silane molecules disssociate as soon as they enter the cavity region, it is reasonable to believe that if the deposition chamber were placed at the side where the silane gas enters the cavity, then silicon could be deposited on the substrates. In fact, the diffusion of the plasma species is symmetric, and their thermal velocity (typically 10^4 cm/sec) is much higher than the flow velocity of the gas stream (at a flow of 100 sccm and a pressure of 0.1 torr, the gas stream velocity is around 90 cm/sec). Then, it is not surprising to observe silicon deposition in the discharge tube which backstreams the gas flow direction.

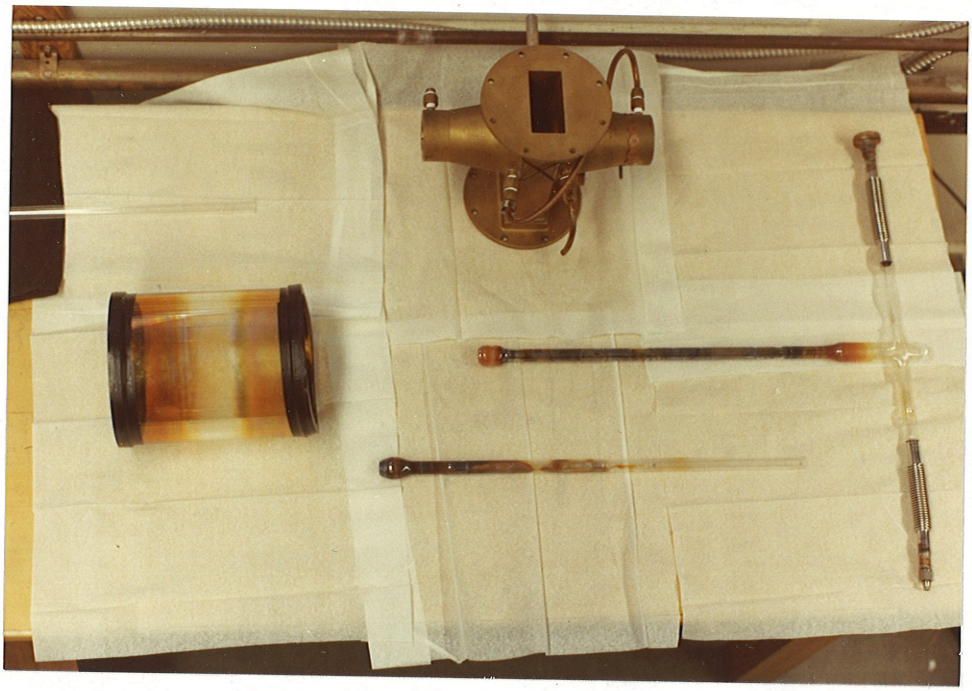

Figure 3.4: Cavity, discharge tubes, and pyrex chamber.

3.2 DISCHARGE TUBE-CHAMBER CONFIGURATION II.

In this configuration the gas mixture was fed to the deposition chamber as shown in Fig. 3.5. Substrates were placed on a holder facing the discharge tube and the cavity as shown photographically in Figs. 3.6 and 3.7. Figure 3.8 shows also photographically a partial view of this configuration including the chamber mounted on an optical bench, part of the gas network, the flowmeters, valves, and the gas inlet to the deposition chamber.

As substrate temperature is known to be an important deposition parameter in controlling the properties of a-Si:H thin films, a substrate heater and thermocouples were incorporated into the deposition chamber, and the substrate temperature could be set and maintained in the range of 25-400 °C. It was not possible to obtain a stable plasma with an arbitrary combination of gas flow rate, pressure, gas mixture, and microwave power. Nevertheless, the microwave power could be varied between 400 and 700 W, and the gas pressure between 0.1 to 0.3 torr.

The best means of controlling the deposition rate was by varying the distance between substrate and discharge tube. Deposition rates were readily controlled between approximatly 50 and 500 Angstroms per minute by this method. An additional factor of importance to the film properties was the invasion of the deposition chamber by the plasma. This was primarily controlled by varying the short circuit at the op-

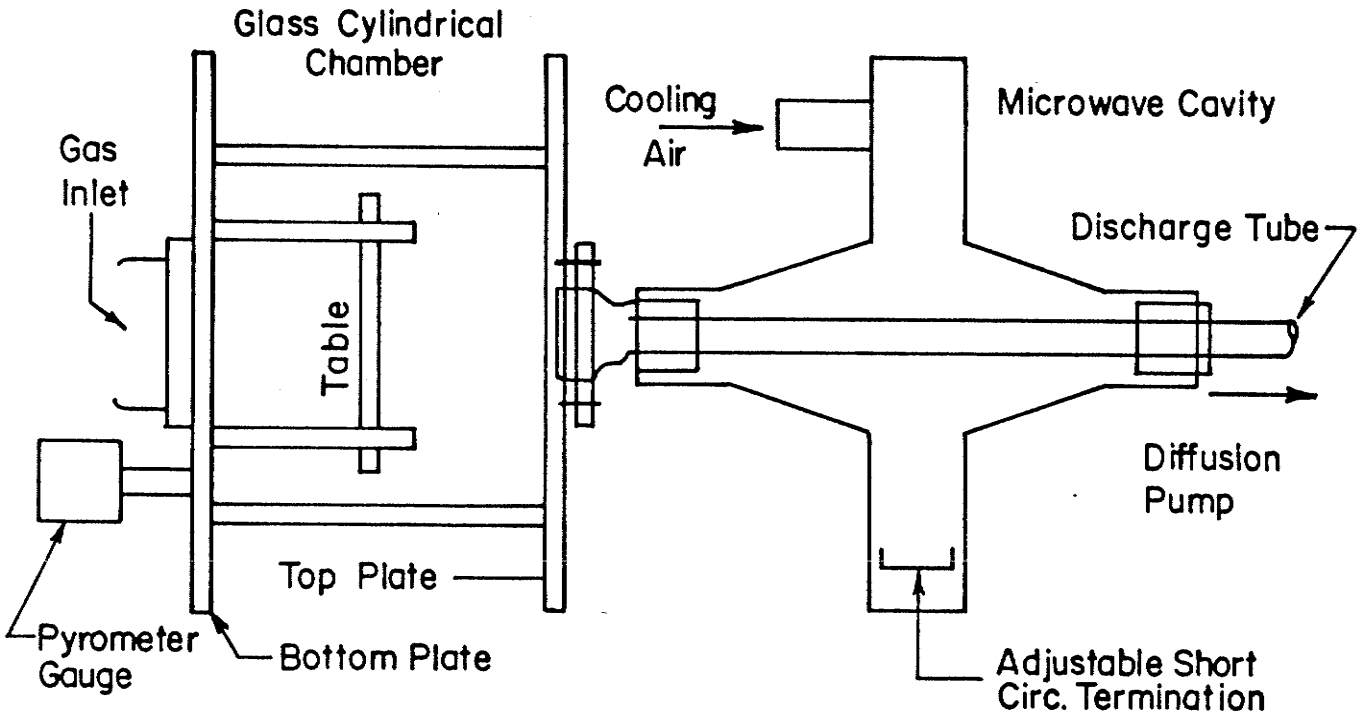

Figure 3.5: Discharge tube-chamber configuration II.

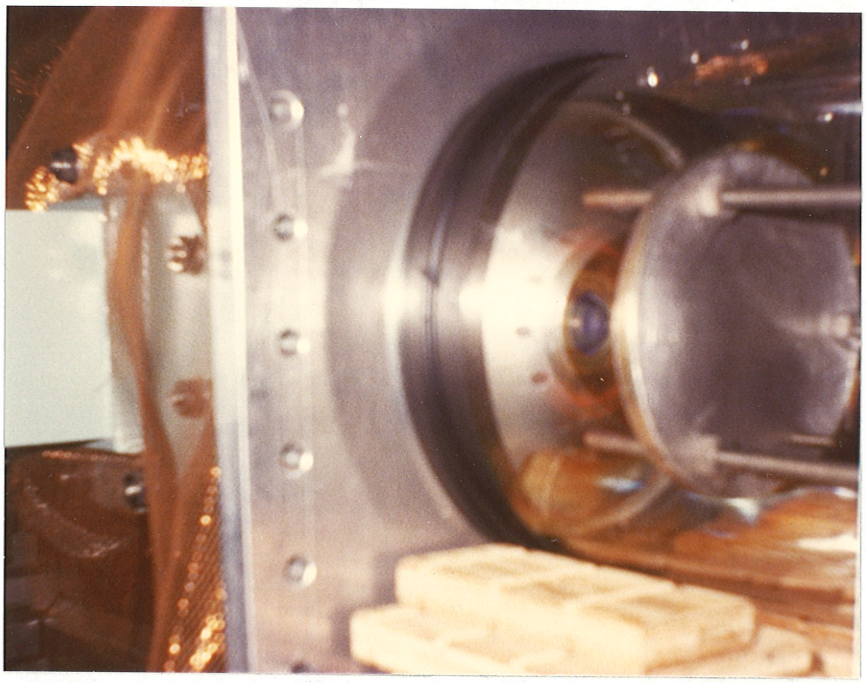

Figure 3.6: The substrate holder facing the plasma glow.

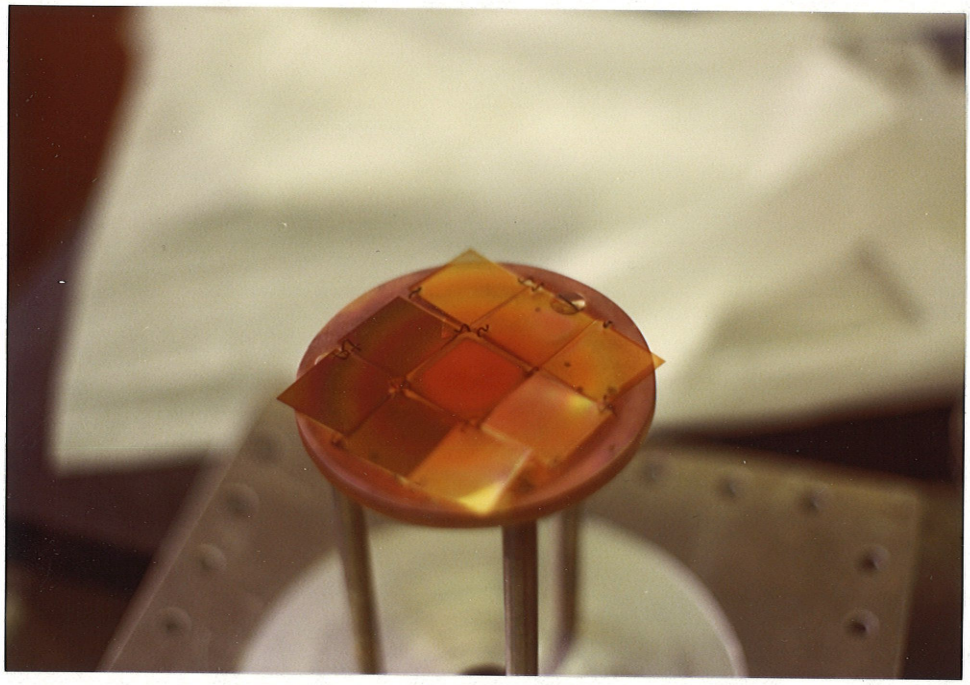

Figure 3.7: A batch of a-Si:H films on the holder.

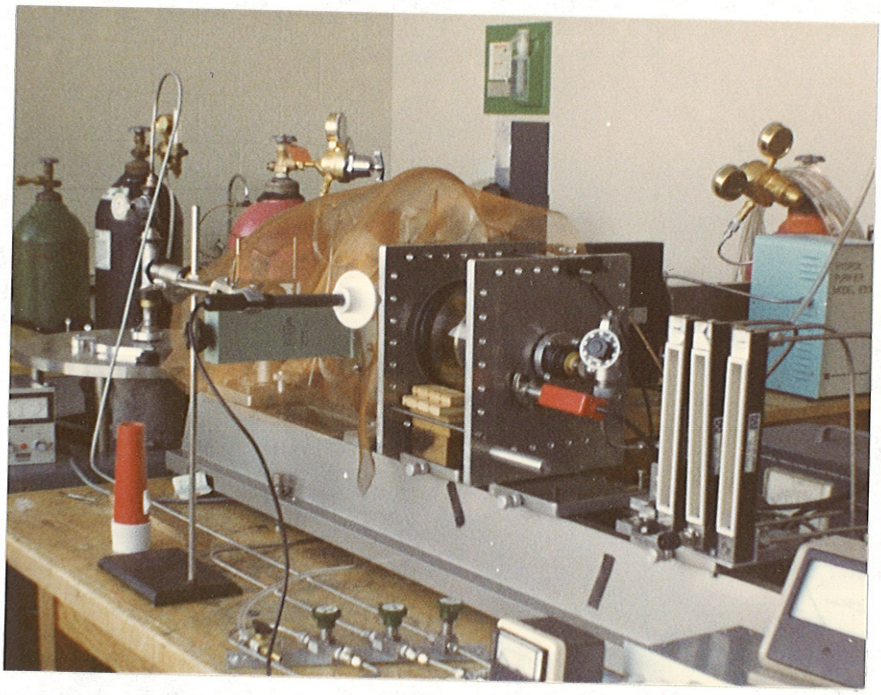

Figure 3.8: The deposition chamber and part of the gas network.

posite end of the cavity, the microwave power, and the gas pressure.

This configuration proved to be satisfactory from the point of view of yielding acceptable deposition rates of a-Si:H films, good thickness uniformity, and structural integrity of the deposited films.

However, the optical and electronic properties of the films, which will be presented in Chapter IV, show consistently large optical gaps, low dark conductivity, and low photoconductivity. These a-Si:H film properties have been correlated to a high oxygen content of the films [38,4,24]. This was originally thought to be due to leaks in the gas-flow system. After all sections of the gas network were carefully checked by means of a helium leak dettector and all vacuum seeals were replaced with new viton seals to ensure no leakage, the oxygen contamination of the silicon films still remained. Later we found that the degree of this contamination was dependent upon the deposition parameters, and in particular, an increase in substrate temperature causes an increase in the oxygen concentration in the films. Also when the plasma was allowed to invade the deposition chamber from the discharge tube as shown in Fig. 3.9, the oxygen concentration was reduced. Based on this clue, the source of oxygen was found to be the microwave plasma etching of the walls of the quartz discharge tube.

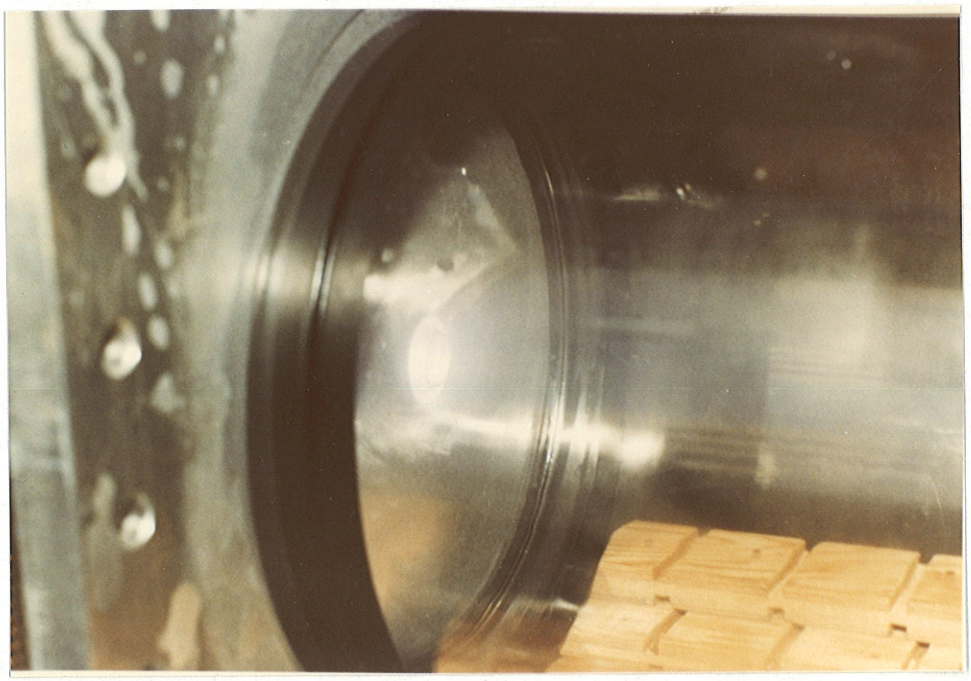

Figure 3.9: The plasma invading the chamber.

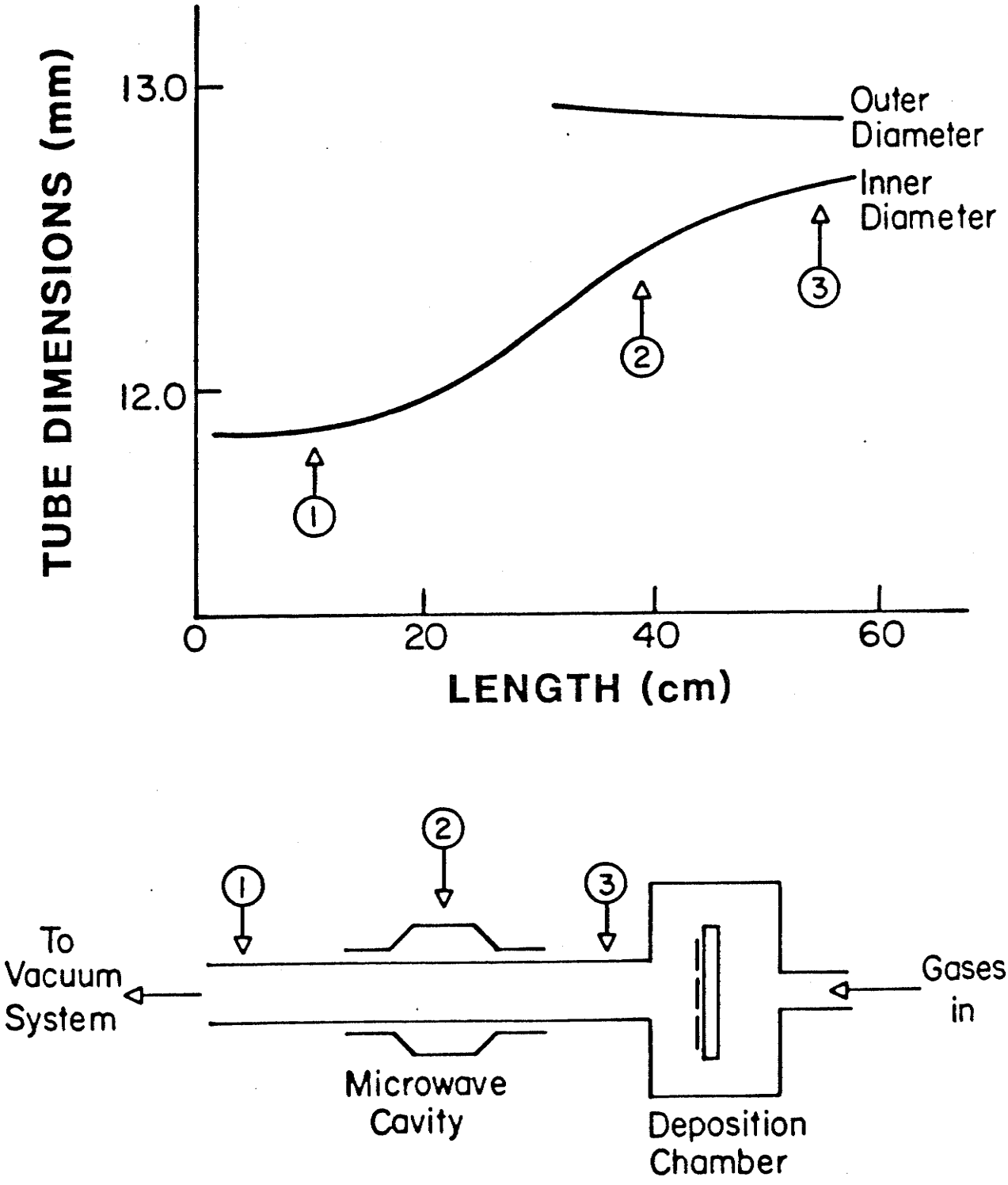

Figure 3.10: Microwave plasma etching of quartz discharge tube.

The evidence for this conclusion is that the tube has been etched non-uniformily along its length, with the maximum etching rate at the deposition end of the microwave cavity as shown in Fig. 3.10. It is believed that the main cause of the plasma etching of the discharge tube is the orientation of the electric field in the coaxial line type microwave cavity. The cylindrical pipe and the plasma in the discharge tube act as the outer and inner conductors of a coaxial line, respectivily. This coaxial cavity is coupled via a cylindrical taper to the H-plane of the waveguide. The electric field that is parallel to the walls of the discharge tube in the waveguide is forced to take a radial direction in the coaxial cavity, thus becoming perpendicular to the discharge tube walls. As the electrons are accelerated along the electric field in the plasma, the most energetic electrons tend to be those travelling in the direction of the electric field, which is perpendicular to the walls of the discharge tube. Kato et al. [19] have measured the radial light intensity distribution for this coaxial line cavity and found a higher electron temperature, or higher electron density, close to the walls of the discharge tube. Taggart [31] has reported for a similar configuration that no sputtering of the discharge tube takes place if the electric field is directed parallel to the walls of the discharge tube, but a piece of silica placed inside the discharge tube soon dissapears in contact with the plasma, and the deposits

could be observed on the walls of the discharge tube. Therefore, plasma etching of the discharge tube turns out to be the fundamental limitation to this system configuration.

One other disadvantage of this configuration is the build-up of silicon deposits on the discharge tube, which absorbs the microwave power, and gives rise to plasma instabilities. The deposition parameters have to be continuously adjusted in order to excite the plasma, while the film grows thicker on the walls of the discharge tube. Eventually, the absorption of the microwave power prevents further excitation of the plasma, and thus prevents further deposition. A solution to the silicon build-up problem on the discharge tube is to insert a thin quartz or stainless steel tube, concentrically with the discharge tube. Kato et al. [20] have reported that by feeding the silane gas into the inner tube and pure argon into the outer discharge tube, the dissociation of silane is prevented from happening in the discharge tube, and thus, the silicon build-up is solved. Although this method may solve the silicon build-up, it enhances the contamination problem by providing a second source of impurities: the inner discharge tube.

3.3 THE SHORT-CIRCUITED WAVEGUIDE CHAMBER CONFIGURATION.

The sputtering of the discharge tube wall places a fundamental limitation upon the use of the discharge tube-chamber configuration for MPCVD of pure semiconductors. The microwave power ranged from 400 to 700 W for maintaining a stable plasma condition. Most of this power either goes to heating of the apparatus, or is radiated to the surroundings, including the operators of the system. The level of radiated microwave power reached up to 10 mW/cm , making the system quite unsafe. The fluctuations of the plasma conditions forced the operators to re-adjust the tuning of the cavity, and thus, expose themselves to high microwave radiation levels.

For all the reasons mentioned above we have developed a new system configuration which solves the problems of the discharge tube-chamber configuration. Preliminary experimental data shows some desirable features. A prototype of this system, referred to as the "short-circuited waveguide chamber" configuration, is shown schematically in Fig. 3.11 and photographically in Figs. 3.12. It is basically a 12 inches long, type WR-284 waveguide, vacuum sealed at both ends by two quartz windows. One of the windows is used for feeding the microwave power into the chamber, and the other for visual observation of the plasma and for OES studies. The waveguide chamber is short circuited by a copper mesh fine enough to prevent any power from being radiated and not to

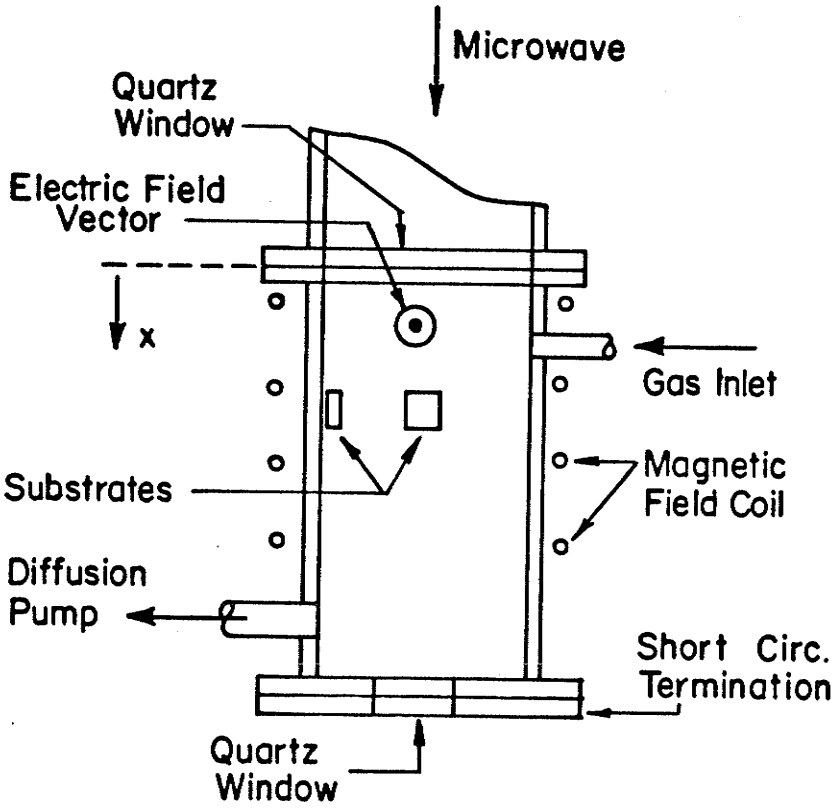

Figure 3.11: Short-circuited waveguide chamber configuration.

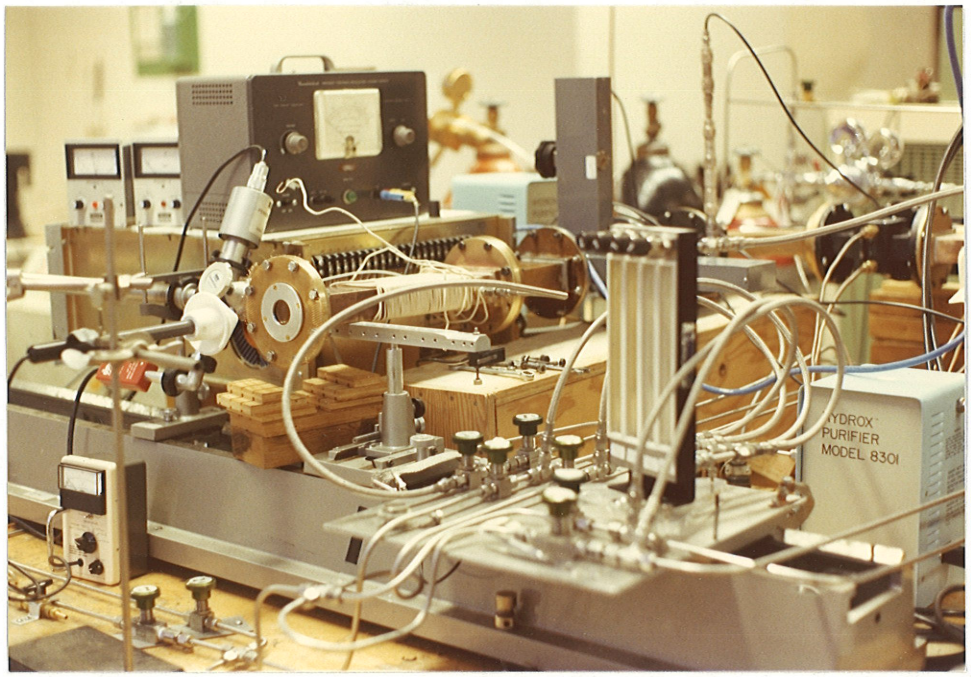

Figure 3.12: Preliminary version of the waveguide chamber.

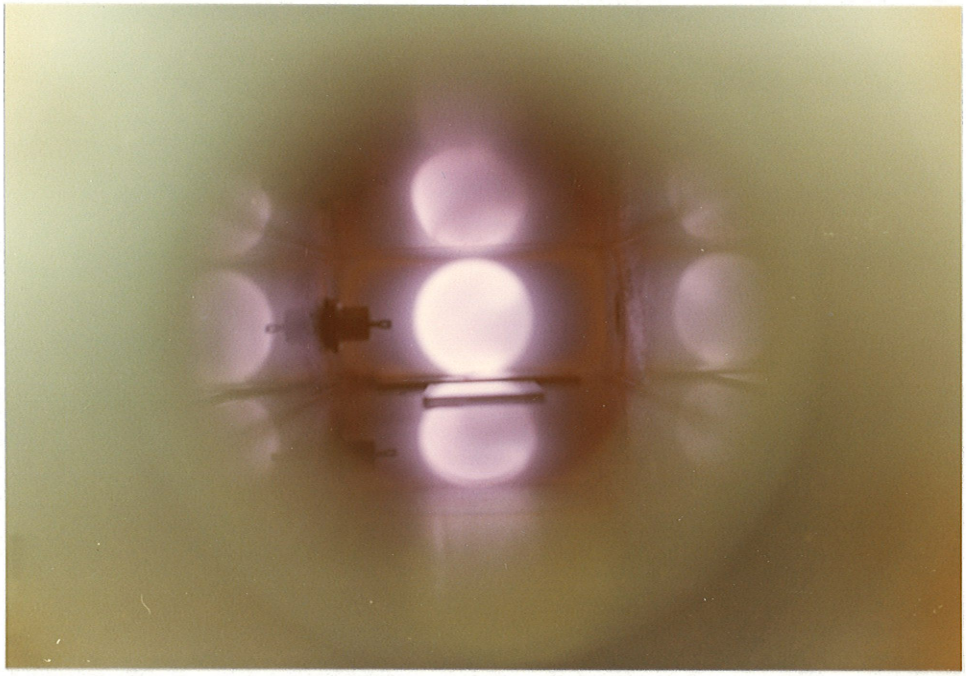

Figure 3.13: A view of silane plasma in the waveguide chamber.

disturb the OES of the plasma. Figure 3.13 shows a view of the plasma through the quartz window and the short-circuiting mesh. A gas inlet port, a vacuum port, and an electric feedthrough are fitted to the E-side of the chamber. The chamber can be baked up to 200 °C with an external electric heater attached to the H-side of the chamber. A magnetic field can be applied along the axis of the chamber by a coaxially mounted coil to confine the plasma and reduce the bombardment of the growing film by energetic electrons, as well as to reduce the sputtering of the chamber walls. This system operates at a microwave power of 10 W, which is more than an order of magnitude lower than that required for the discharge tube-chamber configuration. The short-circuited waveguide chamber configuration also allows the substrates to be placed with their surfaces either parallel or normal to the direction of the electric field in the waveguide operating in the TE_{10} mode.

Hydrogenated amorphous silicon films have been deposited that show reasonable thickness uniformity and optical and electronic properties, which will be discussed in Chapter IV. Of course further improvements of the system to optimize all deposition parameters may show some special advantages of this new microwave deposition technique over the conventional rf glow discharge CVD systems.

Chapter IV

THE EFFECTS OF DEPOSITION PARAMETERS ON THE PROPERTIES

OF HYDROGENATED AMORPHOUS SILICON FILMS.

Hydrogenated amorphous silicon films have been fabricated by the decomposition of silane gas in a dc or rf glow discharge. However, several attempts have been made to fabricate these alloy films at microwave frequencies. At such high frequencies, the plasma constituents would no longer be able to follow the electric field oscillations. To the best of our knowledge, the films have powdery aspects, low photoconductivities, and very high impurity contents [9]. X-ray microanalysis of the deposited films, OES of plasmas, and etching of the structures by the plasma yield evidence of the sources of contaminants in two distinct microwave generator- deposition chamber configurations. The optical and electronic properties of the films fabricated using the configurations discussed in the previous chapter are consistent with the contaminants detected, and show dramatic improvements when the microwave power is reduced and the plasma is confined by a dc magnetic field. Film samples prepared using the second configuration, the short-circuited waveguide chamber, reveal a film quality comparable to that of rf glow discharge deposited films. Preliminary studies on

films deposited using the short- circuited waveguide chamber, on substrates with their surfaces parallel to the electric field (vertical samples, or V) and normal to the electric field (horizontal samples, or H) have different optical, electrical, morphological, and compositional properties . A definite advantage of microwave plasma excitation over dc or rf excitation appears to be a very much faster deposition rate.

4.1 CHARACTERIZATION TECHNIQUES.

The optical, electronic, and morphological properties of the films have been investigated by the following techniques.

1. The transmission spectrum was measured with a Cary 14 spectrophotometer which has the following features: wavelength range, 300-2600 nm; resolution, 3 Angstroms; and reproducibility, within 0.5 Angstroms. From the transmission spectrum the absorption coefficient, optical gap, B value, E_{04} value, and film thickness were determined.
2. Dark conductivity and photoconductivity were measured using a Keithley 602C electrometer.
3. The uniformity and homogeneity of the surface and the cross-section of the films were studied by means of an ISI model II scanning electronic microscope (SEM) with a Robinson backscattered detector, and a charge free anticontamination unit.

4. The impurity concentrations in the films were measured with a PGT System III, energy dispersive x-ray microanalyzer in conjunction with the SEM, which is capable of detecting impurities with atomic number higher than 9, in concentrations greater than 0.19%.
5. The structure of the films was examined by means of a Phillips x-ray diffraction system with a chromium target and a divergent slit of one degree.
6. The absorption spectrum in the infrared was measured using a Nicolet Fourier Transform Infrared Spectrophotometer. From these data hydrogen and oxygen incorporation in the deposited films were determined.
7. Optical Emission Spectrometry (OES) of the plasma was monitored and recorded during deposition to ensure the reproducibility of the deposition conditions, and to detect traces of impurities sputtered from the chamber structures, contaminants in the gas phase, and various species of the plasma chemistry.
8. A Gaertner type L119 ellipsometer and a model L135W Babinet-Soleil compensator were used in conjunction with a Bausch-Lomb grating monochromator and a xenon light source for the measurements of the complex refractive index of the films.

4.2 PHYSICAL PROPERTIES OF THE FILMS.

Thickness uniformity. Films fabricated by both configurations exhibited good thickness uniformity and structural integrity, as shown photographically in Fig. 3.7 for the discharge tube-chamber configuration, and in Fig. 4.18 for the waveguide chamber. The films also exhibited excellent adherence to the substrate for metallic, glass, crystalline Si, and polyethylene substrates.

Film structure. The structure of the films was confirmed to be amorphous by x-ray diffraction . Typical results for a-Si:H are given in Fig. 4.1. This radial distribution function is typical of amorphous structures.

Gross contamination. The results from energy dispersive x-ray microanalysis of the first batch of films deposited by the chamber-discharge tube configuration show clearly that a number of impurities are present in the film, notably aluminum as shown in Fig. 4.2. The aluminum impurities may be due to sputtering of aluminum components of the deposition chamber by the microwave plasma. However, after replacing all undesirable metallic components in the chamber with stainless steel parts, and with microwave power reduced, the concentrations of contaminants were reduced to a level undetectable by the x-ray microanalyzer. It should be noted that the energy dispersive x-ray analyzer was incapable of detecting impurities with atomic number smaller than 9, and we had to use the IR spectrophotometry for the detection of oxygen contamination and hydrogen incorporation in the films.

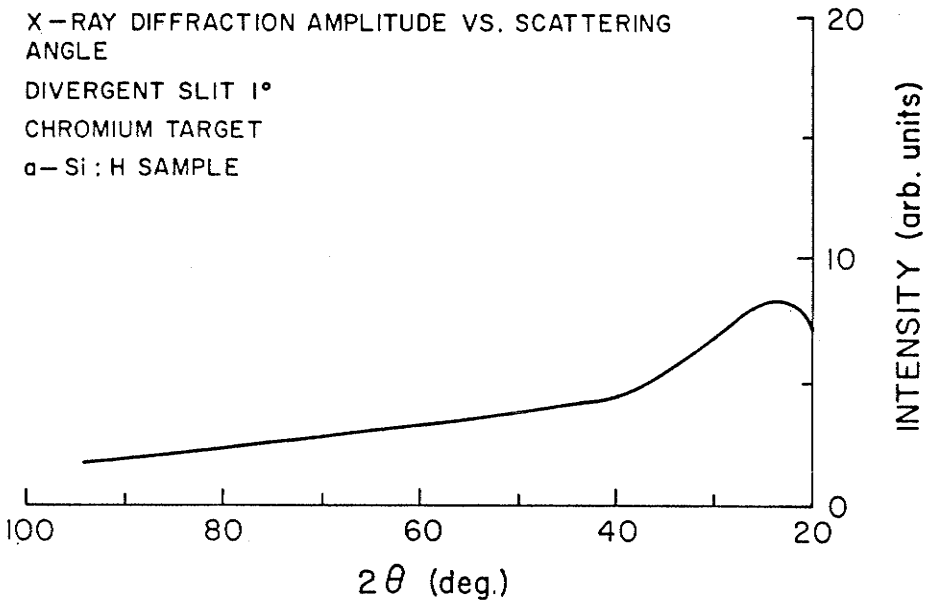

Figure 4.1: Typical x-ray diffraction of a-Si:H films.

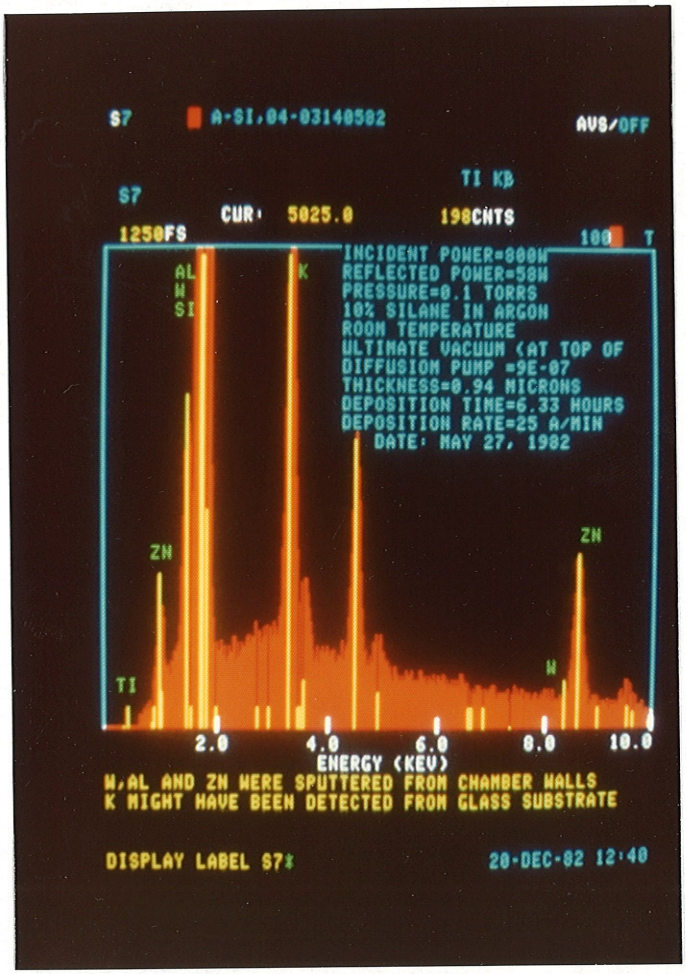

Figure 4.2: Composition of first batch of a-Si:H films.

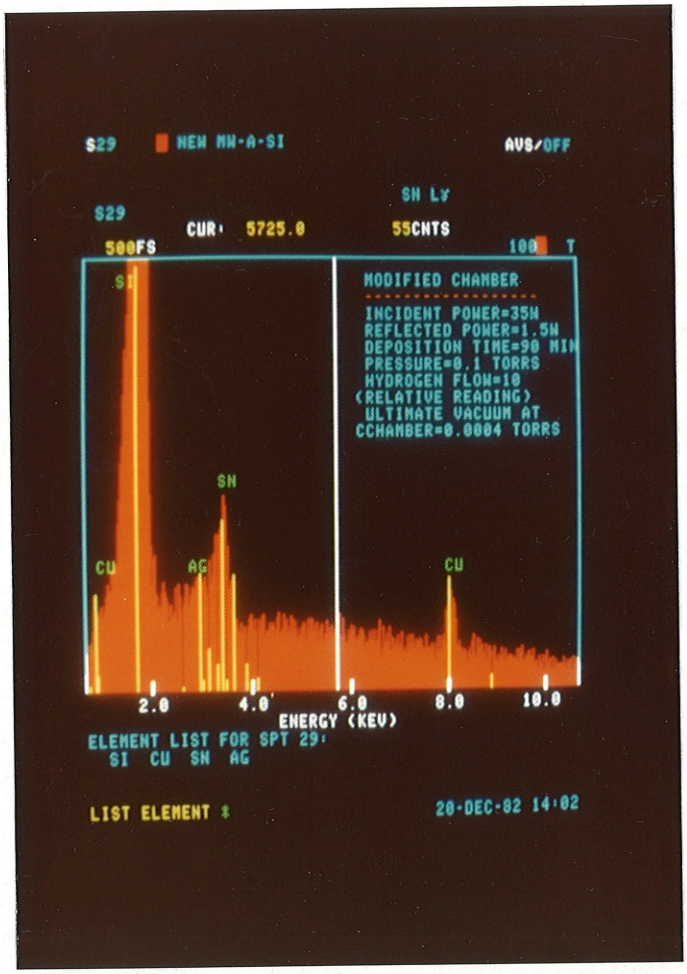

Figure 4.3: Composition of a-Si:H film showing Cu contamination.

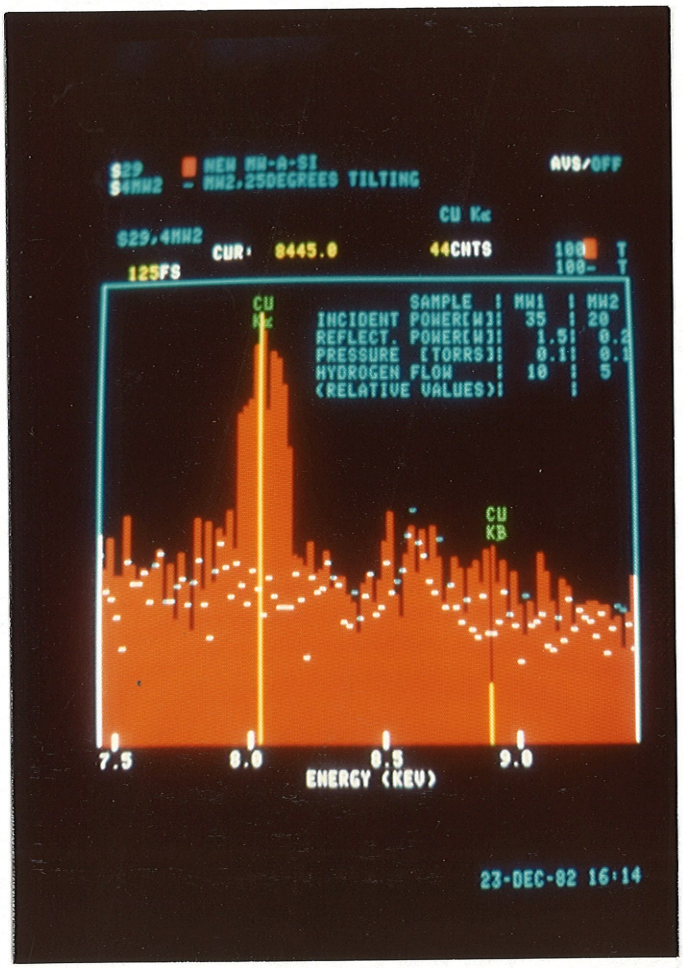

Figure 4.4: Cu traces are eliminated from the a-Si:H films.

In the short-circuited waveguide chamber configuration, the oxygen content of the films was reduced to a level undetectable by OES of the plasma, but oxygen was still observable in the IR spectrophotometry of the films. Nevertheless, the films were very much improved based on the results of dark conductivity and photoconductivity. These films were deposited with microwave powers one order of magnitude lower than in the chamber-discharge tube configuration. However, in the first batch of the films copper appeared to be the primary impurity as shown in Fig. 4.3. With subsequent depositions the copper contamination was not detectable by x-ray microanalysis, as shown in Fig. 4.4 because the waveguide chamber became coated with silicon from preceding runs. It should be noted that copper was also detected by the OES of the plasma during the deposition of the first batch of the a-Si:H films.

It should be mentioned that x-ray microanalyses of our microwave films have never revealed the presence of argon in the films, which we have readily detected in sputtered a-Si:H. The reason for this difference is not known at the present time. Argon was not incorporated in microwave deposited films, even when the gas stream composition was 90% argon, and 10% silane, by volume.

Morphology of the films. Films prepared by the chamber-discharge tube configuration showed a general smooth fracture surface, and elsewhere, evidence of fracture similar to that

seen in glasses. The films prepared by the microwave chamber had morphologies depending on the orientation of the substrates surface with respect to the electric field vector. The films grown with their surfaces normal to the electric field vector exhibited marked columnar growth, while those grown with their surface parallel to the electric field showed a smooth fracture surface. Figs. 4.5 and 4.6 show typical SEM cross-section pictures of these two kinds of film samples.

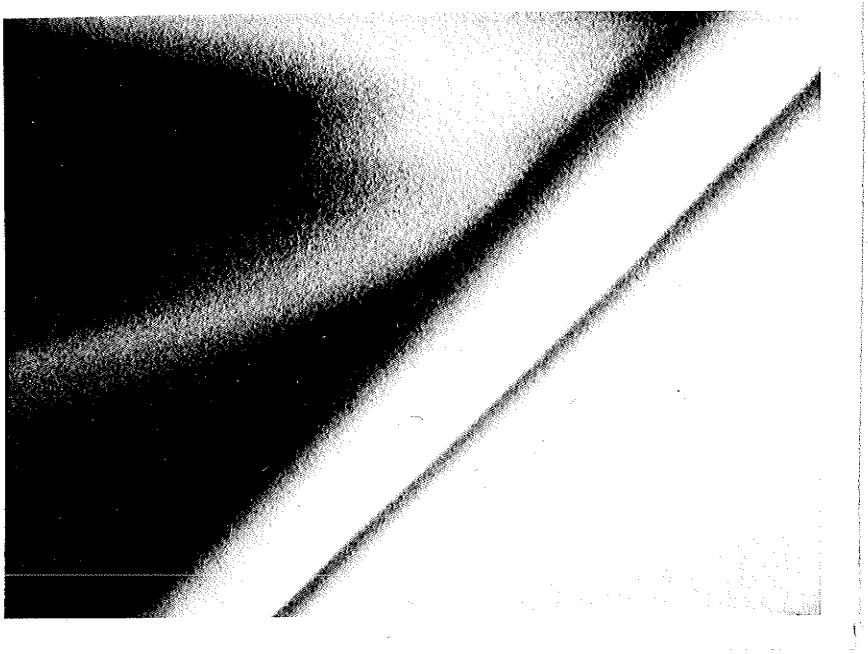

Figure 4.5: Smooth cross-section of a V-type a-Si:H film sample.

Figure 4.6: Columnar growth in H-type a-Si:H film sample.

4.3 DEPOSITION CHAMBER-DISCHARGE TUBE CONFIGURATION.

4.3.1 Experimental conditions.

Films have been deposited under a wide variety of deposition conditions; microwave power ranged from 400 to 700 W, gas pressure 0.1 to 0.25 torr, gas composition of silane/hydrogen in argon from 1/1 to 1/4, substrate temperature from 25 to 245 °C, distance from substrate holder to discharge tube end 3 to 14 cm. As has been reported in Chapter 3, the build-up of silicon deposits on the discharge tube made it necessary to increase the microwave power, during the deposition period, in order to excite the plasma. When the deposited film on the discharge tube became so thick that the microwave power could not be transmitted through it at sufficient power levels to excite the plasma, the deposition process was brought to an end. This constant change of the power forced changes in other deposition conditions such as the flow and the pressure. Thus, the effects of each deposition condition was difficult to assess, except for a few of these conditions, such as microwave power range, substrate temperature, gas mixture composition, and discharge tube end to substrate distance.

4.3.2 Optical properties of the films.

The techniques employed for optical characterization of the a-Si:H films were spectrally-resolved ellipsometry, visible-near infrared spectrophotometry, IR spectrophotometry, and

high-resolution far-infrared spectrophotometry. A description of these investigations, the methods used and representative results obtained are given below.

Spectrally resolved ellipsometry measurements. The complex refractive index has been measured with an ellipsometer in the range 350 to 1000 nm. This range covers the photon energies larger and smaller than the optical band gap. The ellipsometric measurements were made by null setting the polarizer and analyzer which gave two characteristic parameters, Δ defined as the phase angle change, and Ψ defined as the arctangent of the amplitude ratio change between the two components of polarization upon reflection [3]. In such measurements we could have only two measured parameters, but there are three unknown constants which are the refractive index n, the extinction coefficient k, and the film thickness d. Thus, to enable the computation for n and k we have to estimate the value of d.

The film thickness was estimated by the following methods:

1. It was measured by observing the cross section of the film with a SEM, having the cross-section of the film normal to the electron beam. The magnification of the SEM was properly calibrated by using a calibration standard pattern of 2160 lines per milimeter. This method was useful for thicknesses greater than 0.5 microns, since the error is smaller than 10%.

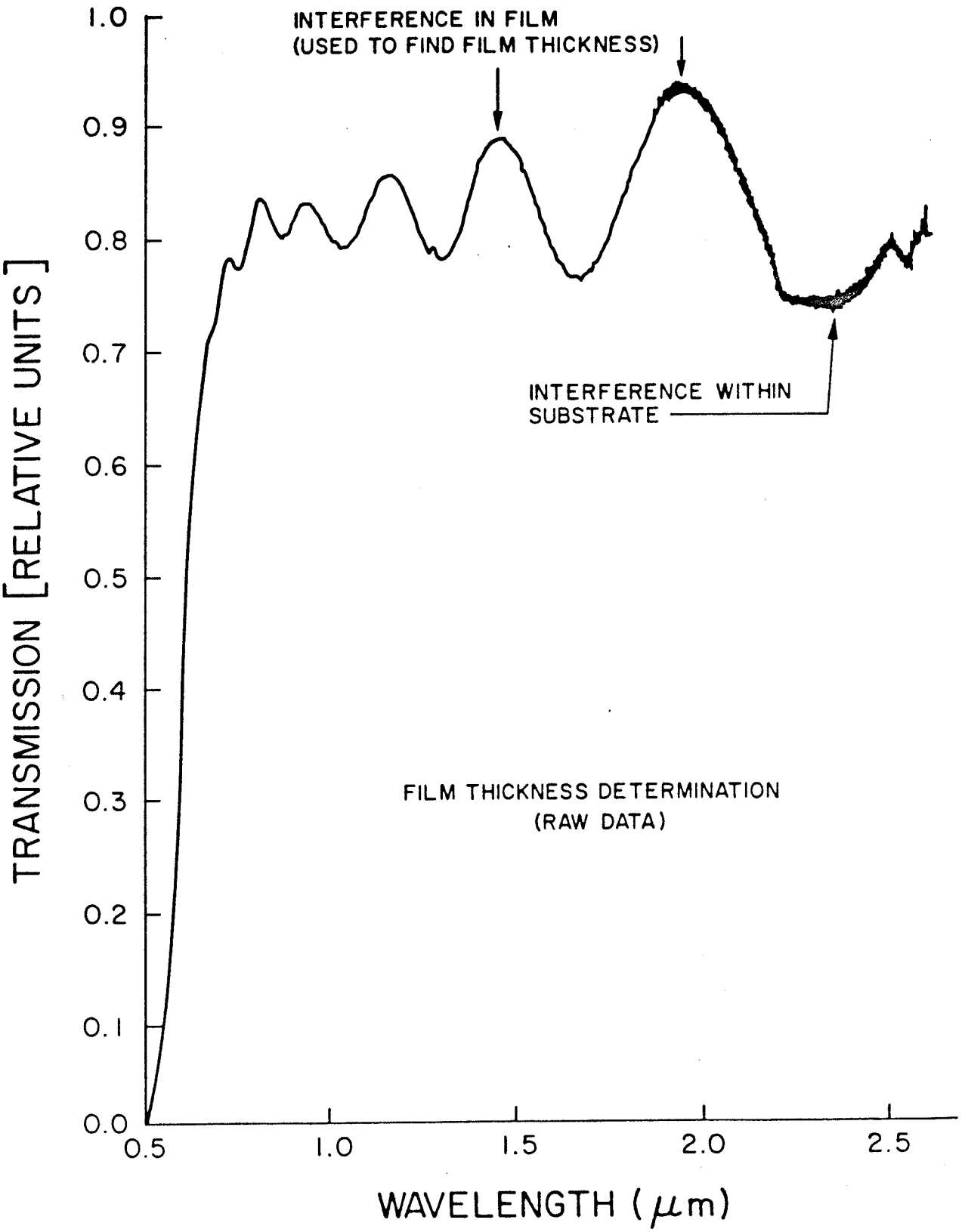

Figure 4.7: Typical near infrared interference frindges of a-Si:H films.

2. It was estimated by weighing the substrate before and after the film deposition and calculated from the density of the films.
3. At wavelengths much longer than the optical transmission cutoff wavelength, the absorption is small and the light would traverse the sample several times causing interference fringes which results in maxima and minima of the total transmitted light intensity. A typical example for an a-Si:H film prepared by the chamber-discharge tube configuration is shown in Fig. 4.7. The film thickness and hence the refractive index can be determined on the basis of the condition for the occurrence of such extremum values of transmission. For two successive interference maxima, the wavelengths for maxima satisfy

$$(1/2)\ m\ \lambda = 2\ n\ d \qquad (4.1)$$

and those for minima satisfy

$$(1/2)(\ m + 1\ )\ \lambda = 2\ n\ d \qquad (4.2)$$

where m is an even integer. These equations are valid if k is negligibly small. This assumption was found to be satisfied in the present investigation.

The film thickness estimated by means of these three methods was consistent. With this estimated value of d and

the measured values of Δ and Ψ , a Fortran computer program [30,1] was used to yield accurate values of n, k, and d, by iteratively minimizing the error function.

In this investigation, the shortest wavelength that could be used was 350 nm, which was limited by the quality of the optical elements of the ellipsometer, whereas the longest, 1000 nm, was limited by the sensitivity of the Si photodetector. For wavelengths longer than 1000 nm the data were deduced from the interference fringes in the spectrophotometric measurements. All measurements were performed at room temperature in a dark room.

The complex refractive index may be written as

$$n^* = n - ik \qquad (4.3)$$

where the real part n is the refractive index and the imaginary part k is the extinction coefficient.

Typical results for n and k obtained by spectrally resolved ellipsometry are shown in Fig. 4.8. These data were obtained for an a-Si:H film prepared in a gas composition of 10% silane and 90% argon, by volume. The substrate temperature was held at 25 °C during deposition. The optical absorption coefficient may be directly obtained from the extinction coefficient k according to

$$\alpha = 4 \pi k / \lambda \qquad (4.4)$$

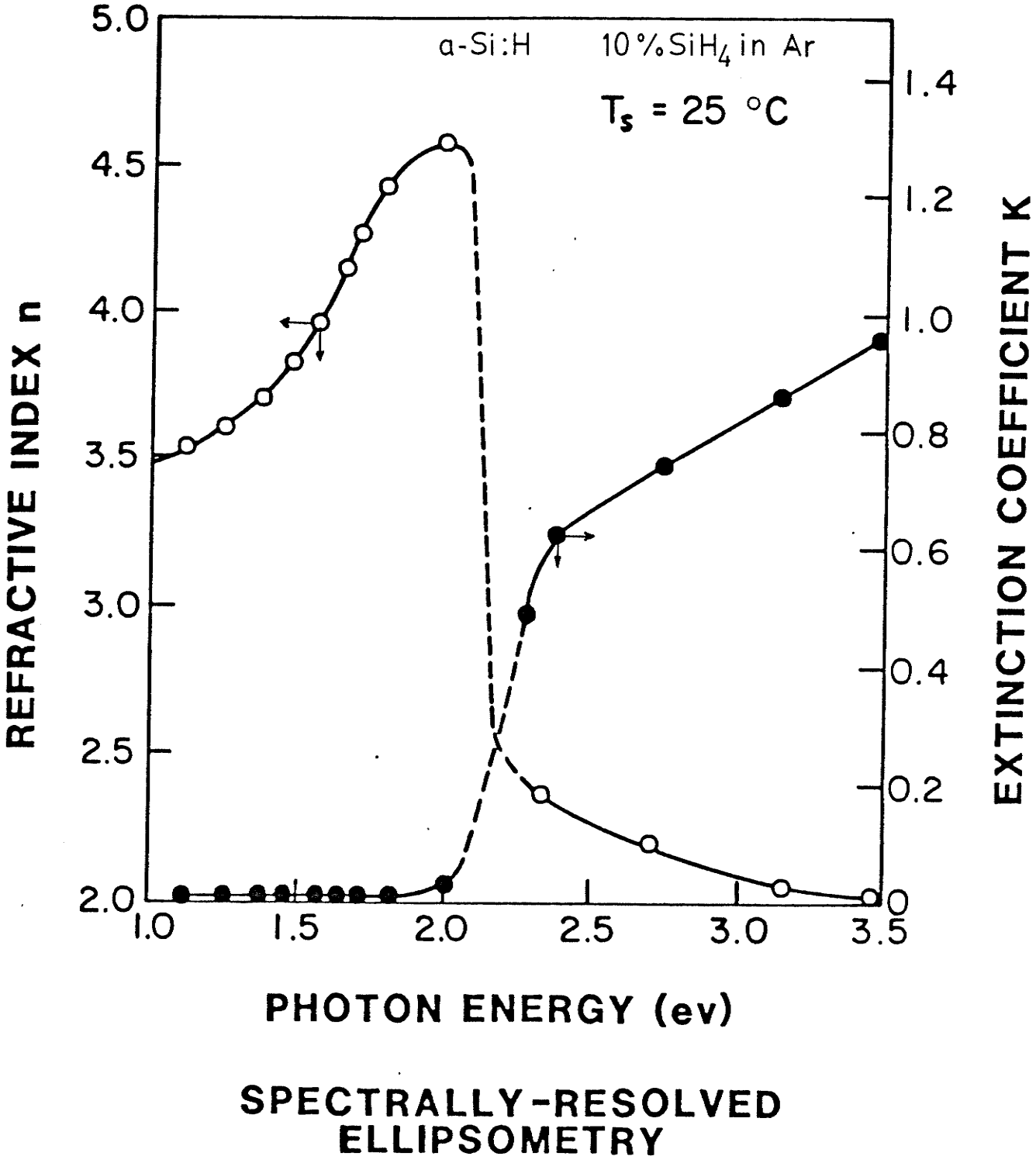

Figure 4.8: Constants n and k as functions of photon energy.

at the wavelength λ. Absorption coefficients obtained by this approach agreed well, within experimental error, with those obtained by direct optical absorption measurements, which are discussed in the following section.

Optical absorption measurements. In crystals, electronic transitions between valence and conduction band have to obey the selection rules based upon k conservation. In the amorphous semiconductor case, where the wave-functions become localized over a certain volume rather than extended over the whole volume of the sample, the disorder produces broadening in k-space. This leads to a relaxation of the k-selection rules that results in a smooth absorption band [43], and localized tail states.

At photon energies in excess of the absorption edge, the optical absorption data obey the following relation

$$\alpha \hbar \nu = B \left(\hbar \nu - E_o \right)^{1/2} \qquad (4.5)$$

where E_o is the optical gap, α is the absorption coefficient and $h\nu$ is the photon energy. The parameter B includes information of the tail states and is strongly influenced by processing conditions. This parameter has been correlated with photoconductivity [36]. This quadratic relationship indicates that the band structure in the neighbourhood of the mobility edge is parabolic [43].

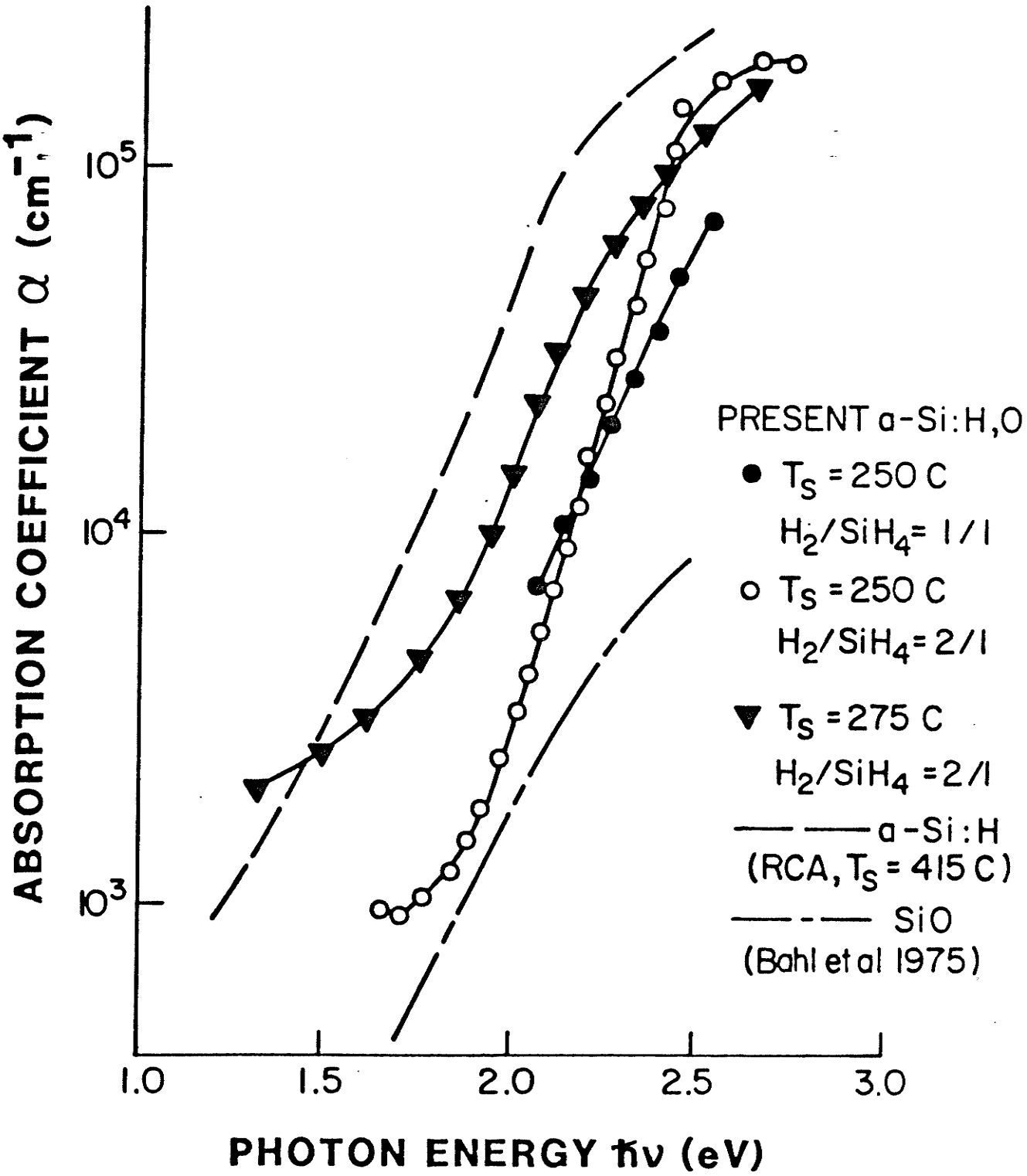

Figure 4.9: Absorption coefficient vs. hν for various films.

Typical experimental results obtained by direct optical absorption measurements, using a Cary-14 scanning spectrophotometer, for a-Si:H films prepared by MPCVD are shown in Fig.4.9. For comparison purposes, the results for a-Si:H films prepared by the rf glow discharge techniques [8] and for a-SiO films reported by Bahl et al. [4] are included. As has been mentioned in previous chapters, a major contaminant in the a-Si:H films prepared by the deposition chamber-discharge tube configuration was oxygen resulting from the sputtering of the quartz discharge tube. This is consistent with the results shown in Fig. 4.9, which show the dependence of α upon $\hbar\nu$ to be intermediate between a-Si:H and a-Si:O films.

In order to extract the B parameter and the optical gap E_o, the results have been replotted in terms of $(\alpha\hbar\nu)^{1/2}$ as a function of $\hbar\nu$, as shown in Fig. 4.10. A film with a low oxygen content will be expected to have a relatively low optical gap E_o. In addition, if the energy extent of the tail states is small, the parameter B will be large. The results presented in Table 4.1 show that a high deposition rate increases B and perhaps also reduces E_o, thereby resulting in a-Si:H films with better properties.

There was no definite correlation between B or E_o and microwave power (except insofar as the power influence on the deposition rate). However, there was an indication that the optical gap increases with increasing substrate tempera-

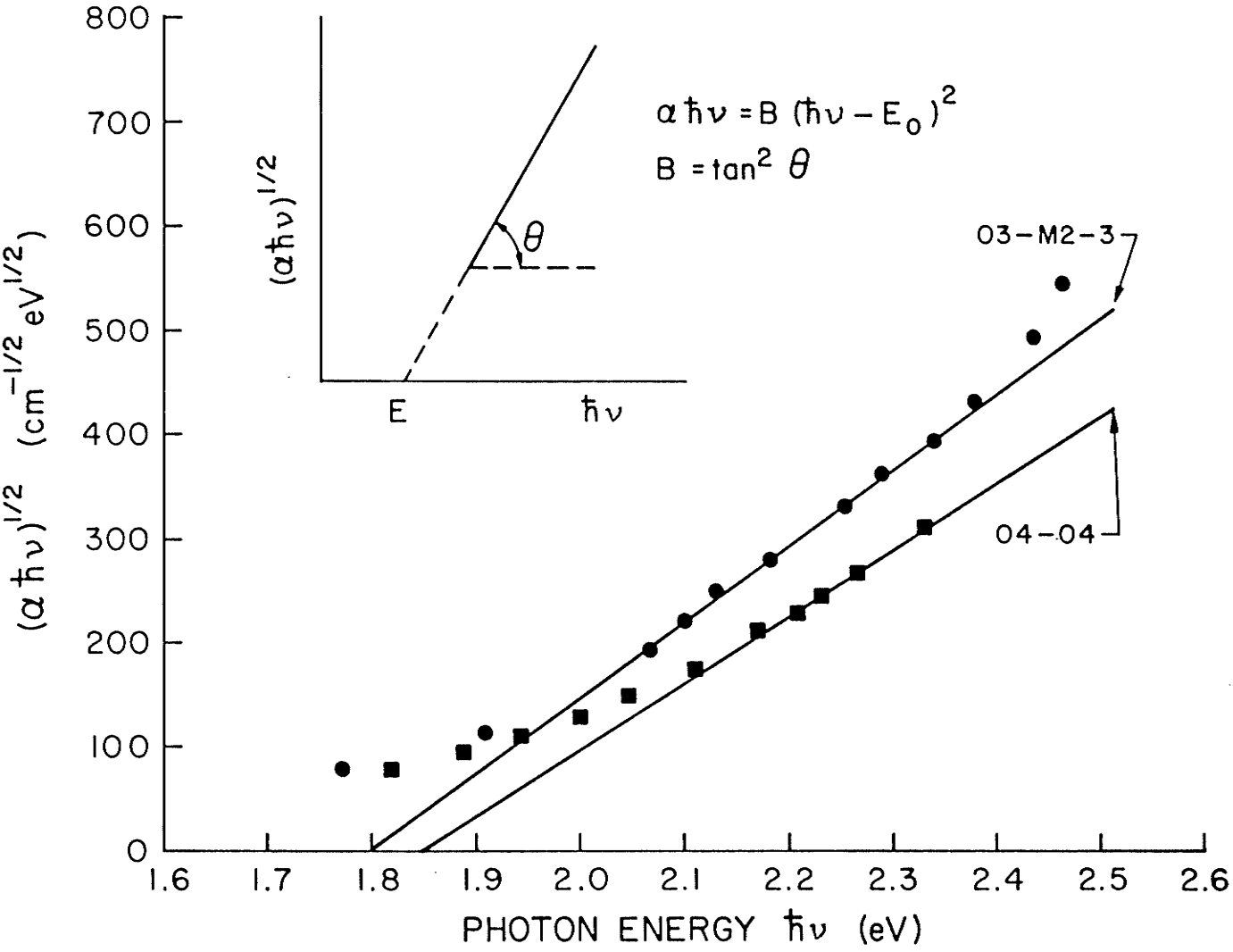

Figure 4.10: The value of $(\alpha\hbar\nu)^{1/2}$ as a function of photon energy.

TABLE 4.1

Optical properties of a-Si:H films.

Deposition Rate (A/min)	E_o (eV)	E^*_{04} (eV)	B (10^{5b} cm^{-1} eV^{-1})
4.9	1.88	2.1	4.09
17.3	2.00	2.1	5.40
26.4	1.84	2.0	5.66
36	1.98	1.98	5.40
65	1.87	1.67	7.30

* E_{04} is defined as the energy for which $\alpha = 10^4$ cm^{-1}.

ture T_s if other conditions remain unchanged. This implies that more oxygen is incorporated in the films at higher T_s. The oxygen contamination has been greatly reduced in the films deposited in the short-circuited waveguide chamber, which will be discussed in section 4.4.

Infrared and far-infrared spectra. In order to measure the infrared and the far-infrared absorption characteristics, the a-Si:H films must be deposited on substrates transparent to the light in the infrared region. Crystalline silicon and polyethylene meet this requirement for the infrared and far-infrared region respectively. Therefore, we used these materias for substrates in these investigations.

Hydrogenated amorphous silicon films were deposited by MPCVD onto high resistivity, intrinsic crystalline silicon wafers of 2 cm in diameter and 1 mm in thickness, and onto 2.5x2.5 cm polyethylene substrates, 0.8 mm in thickness at room temperature in a mixture gas of 10% silane and 90% ar-

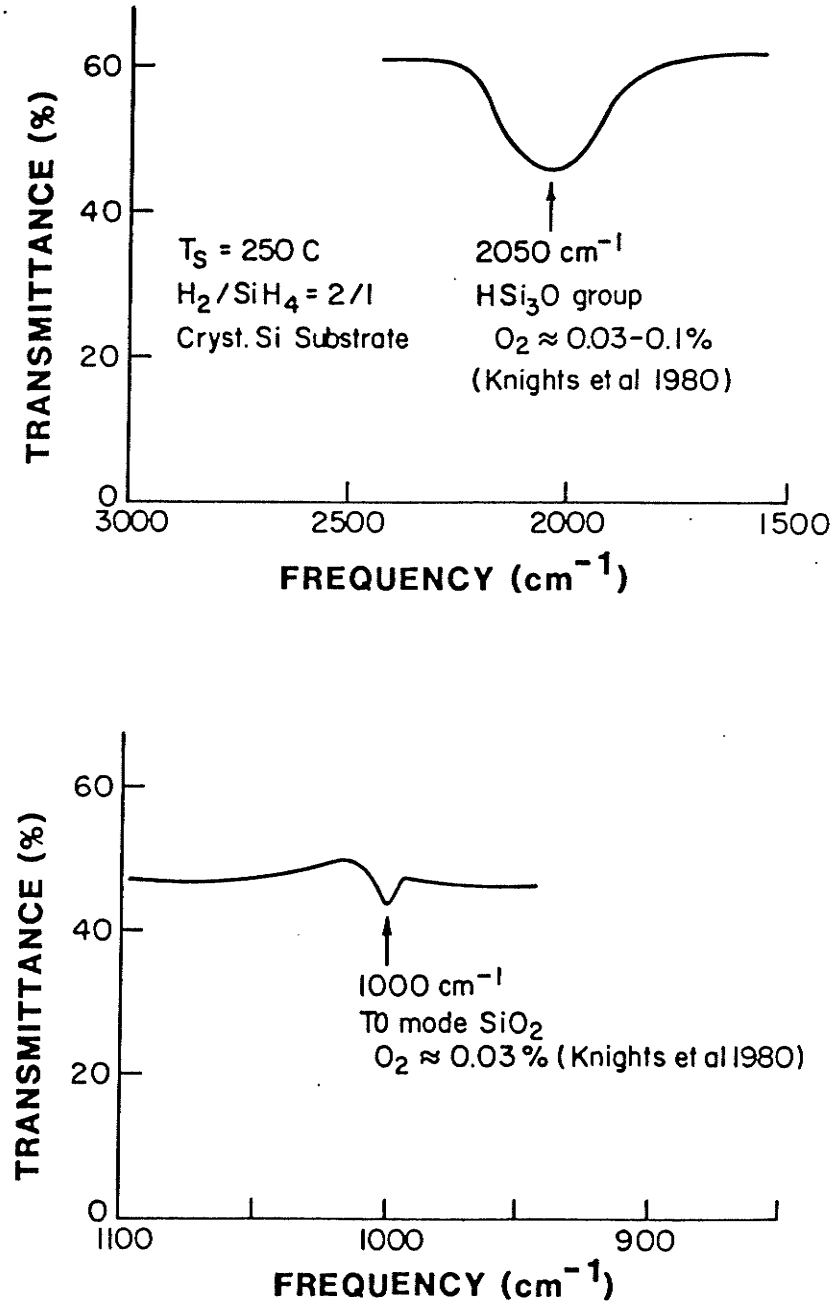

Figure 4.11: Infrared absorption spectra of a-Si:H films.

gon. The films deposited on crystalline silicon wafers were used for the frequency range 400-4000 cm^{-1} . Further evidence of the presence of oxygen in the a-Si:H films was found, as manifested by the absorption around 1000 cm^{-1} , shown in Fig. 4.11. The 1000 cm^{-1} mode is the characteristic transverse optical mode of the SiO_2 network. According to Knights et al. [24], the shift of this peak from 950 cm^{-1} to 1050 cm^{-1} implies an increase of the oxygen concentration. The peak at 1000 cm^{-1} in the lower graph of Fig. 4.11 corresponds to an oxygen concentration in the gas mixture of 0.03%. The oxygen concentration in the a-Si:H films is expected to be much larger. In fact, conventional infrared absorption measurements on thin films will not reveal the presence of oxygen concentrations less than about 1% [4].

The upper part of Fig. 4.11 shows an absorption peak at 2050 cm^{-1} . This peak corresponds to a HSi_3O group and its energy corresponds to a gas-phase oxygen concentration of 0.03 to 0.1% [24], which is consistent with the peak at 1000 cm^{-1} . It should be noted that by comparing their results for E_{04} (defined as the energy at which $\alpha = 10^4$ cm^{-1}) with published data for SiO_x, Knights et al. [24] have concluded that an increase of E_{04} of about 0.6 eV for films deposited in the gas stream with 1% oxygen, corresponds to a composition x of about 0.7, and that the oxygen content in the film is enhanced by one to two orders of magnitude compared to the gas content.

Far-infrared spectra. The far infrared measurements were made on samples with polyethylene substrates using a Nicolet 7199 Fourier-transform far-infrared interferometer with 1 cm^{-1} resolution.

Figures 4.12, 4.13, and 4.14 show the absorbance vs. wavenumbers in the 630-659, 531-57, and 67-90 cm^{-1} regions. The present data confirm the presence of SiH, SiH_2, and SiH_3 bonding configurations in the film, and suggest the possibility of more complex systems. All these three modes should be infrared active in the 630-650 cm^{-1} region [26]. We have been able to accomplish the resolution needed in order to separate the rocking and wagging modes for the SiH_2 and SiH_3 configurations. Lucovsky et al. [26] have identified and estimated the SiH rocking and bending modes to be around 650 cm^{-1}. Therefore, the absorption at 652 cm^{-1} could be attributed to that bonding configuration. But, it could also be a pure bending motion of a Si-O-Si-H configuration involving the motion of the oxygen and hydrogen atoms [27]. The calculated frequency for this mode is 650 cm^{-1}. A pure oxygen bending mode for this configuration has a calculated frequency of 630 cm^{-1}. Lucovsky et al. [27] also find an out-of-plane hydrogen bending mode at 630 cm^{-1}. Thus, the assignment of the 652 and 639 cm^{-1} absorption remain uncertain. Further work, with a contollable amount of oxygen incorporated into the film and with the absorption spectra at the 700-1000 and 2000-2300 cm^{-1} ranges are required in order

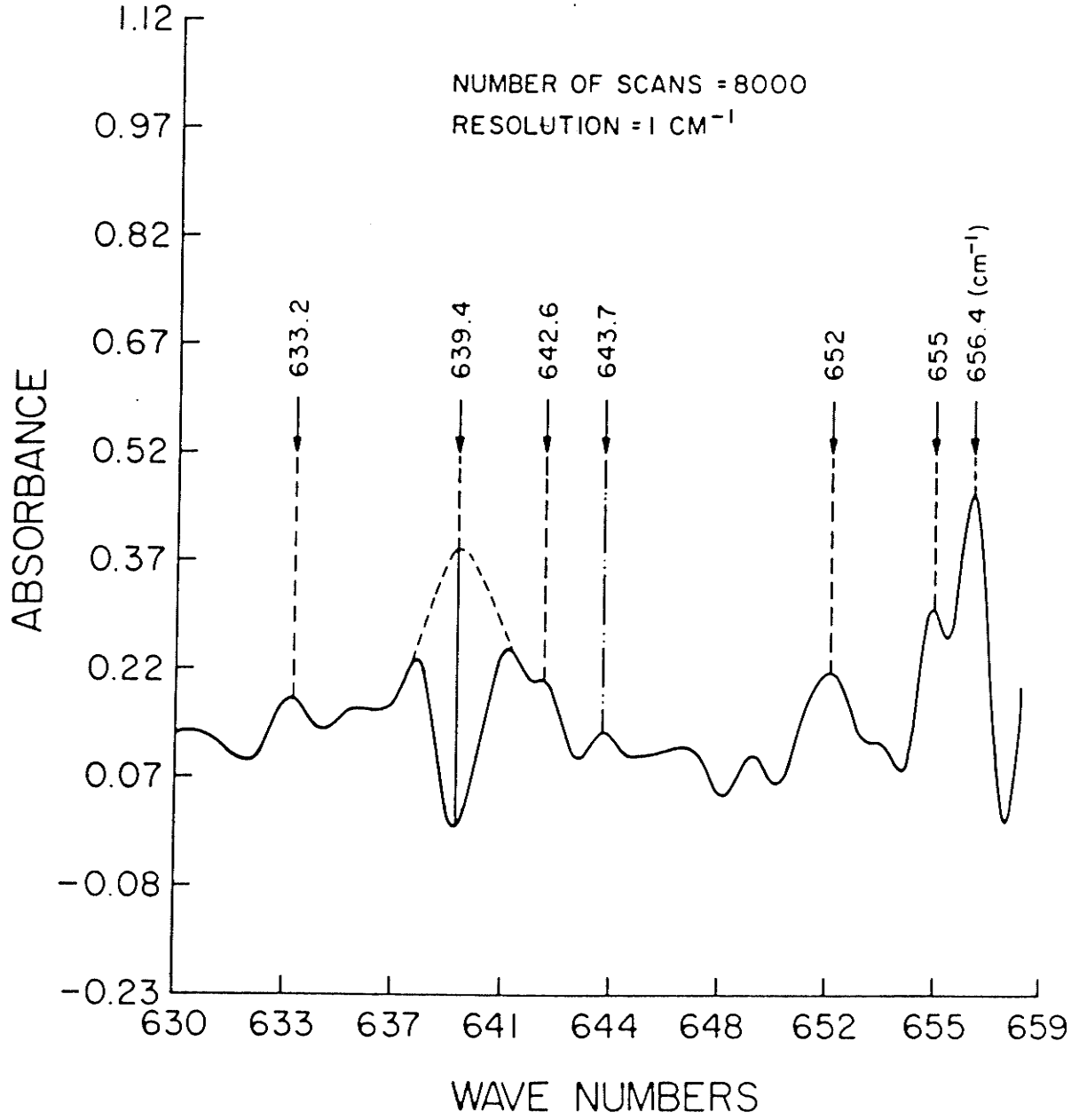

Figure 4.12: Far IR spectrum in the range 630-659 cm^{-1}.

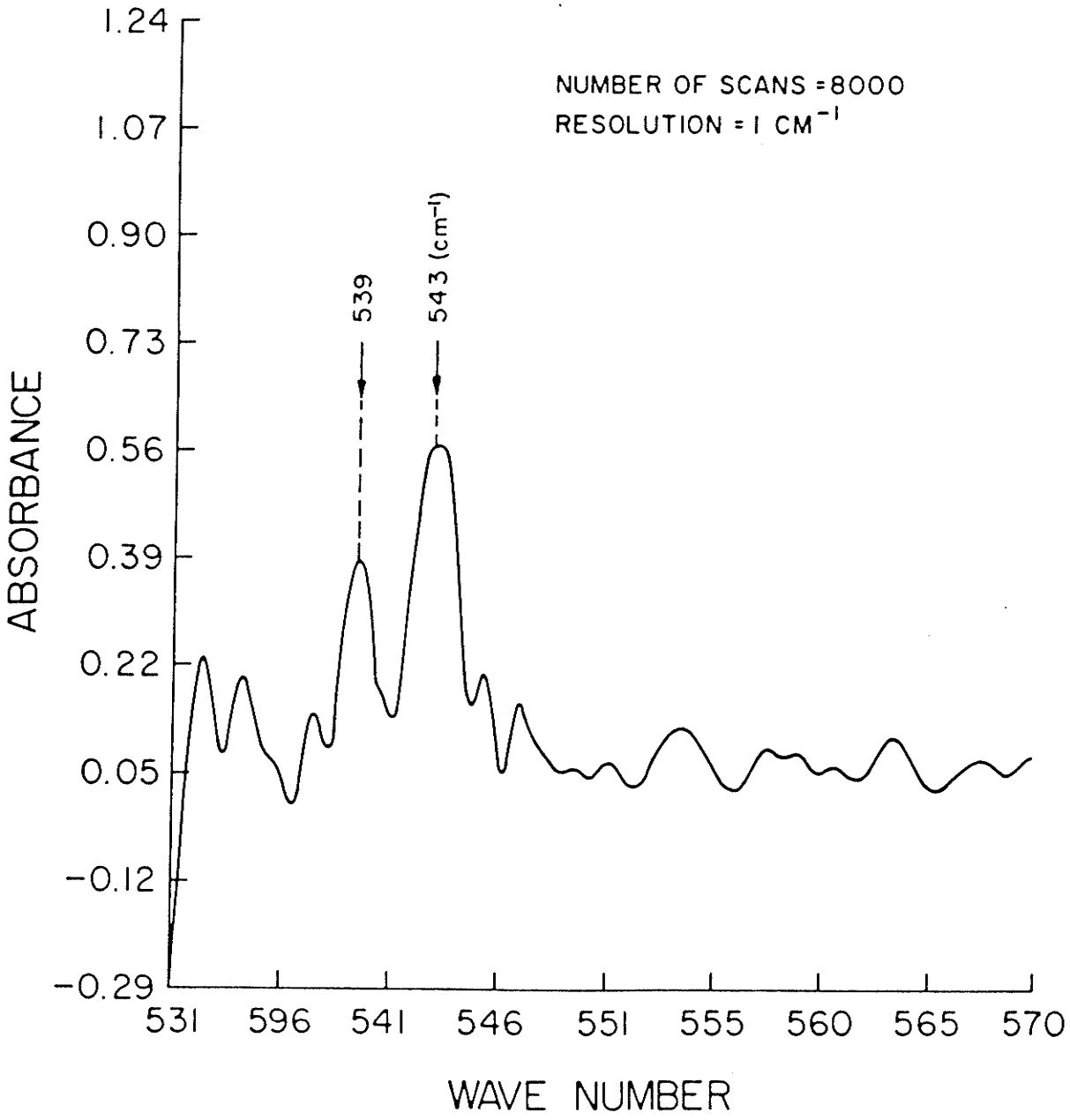

Figure 4.13: Far IR spectrum in the range 531-570 cm^{-1}.

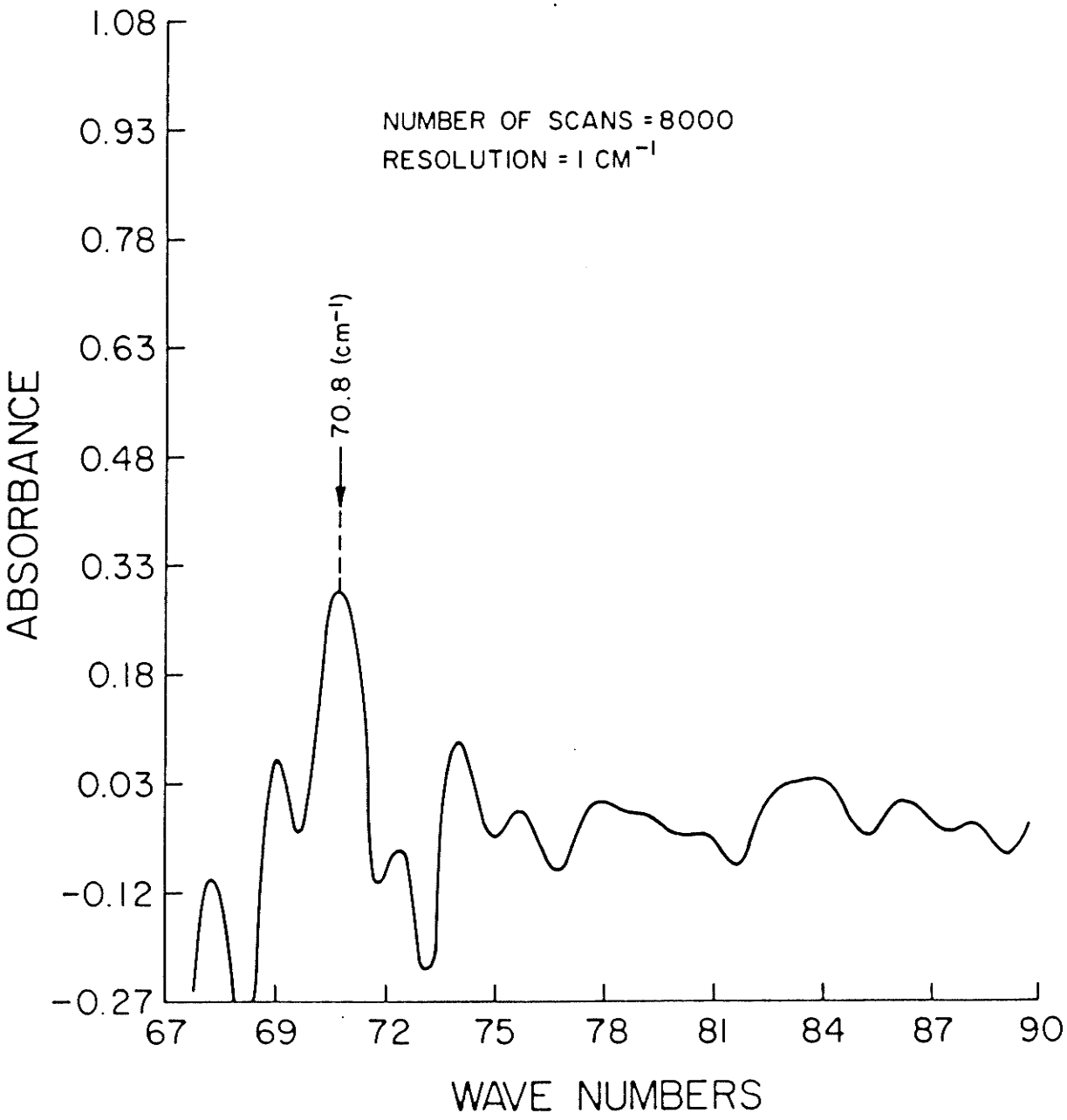

Figure 4.14: Far IR spectrum in the range 67-90 cm^{-1}.

to distinguish and properly assign the absorptions in these infrared regions.

4.3.3 Electronic properties.

Dark conductivity. Dark conduction current as a function of electric field for a variety of film samples, with various metallic electrodes, and deposition temperatures T_s , are shown in Fig. 4.15. The conductivity of the films deposited at lower temperatures (200 and 250 °C) is nearly ohmic, and it is independent of both polarities of the electric field and the nature of the electrode material, in spite of a large difference in work fuctions of these materials, such as Au and Al with a work function difference of 0.8 eV [40]. For the films deposited at the substrate temperature of 275 °C, the dark conductivity is low, this may be due to the oxygen content. These films which have low field conductivity in the order of 10^{-14} $(ohm\text{-}cm)^{-1}$ may be characteristic of involving Si O_x content. They also exhibit a field dependent transport mechanism at high fields as shown in Fig. 4.15.

Temperature dependence of the dark conductivity yields activation energies in the 0.5 to 0.6 eV range. This implies that the conduction is via the extended states, and that the equilibrium Fermi level is located at the level 0.5 to 0.6 eV below the mobility edge of the conduction band [33]. The observed variation in activation energy of the dark conduc-

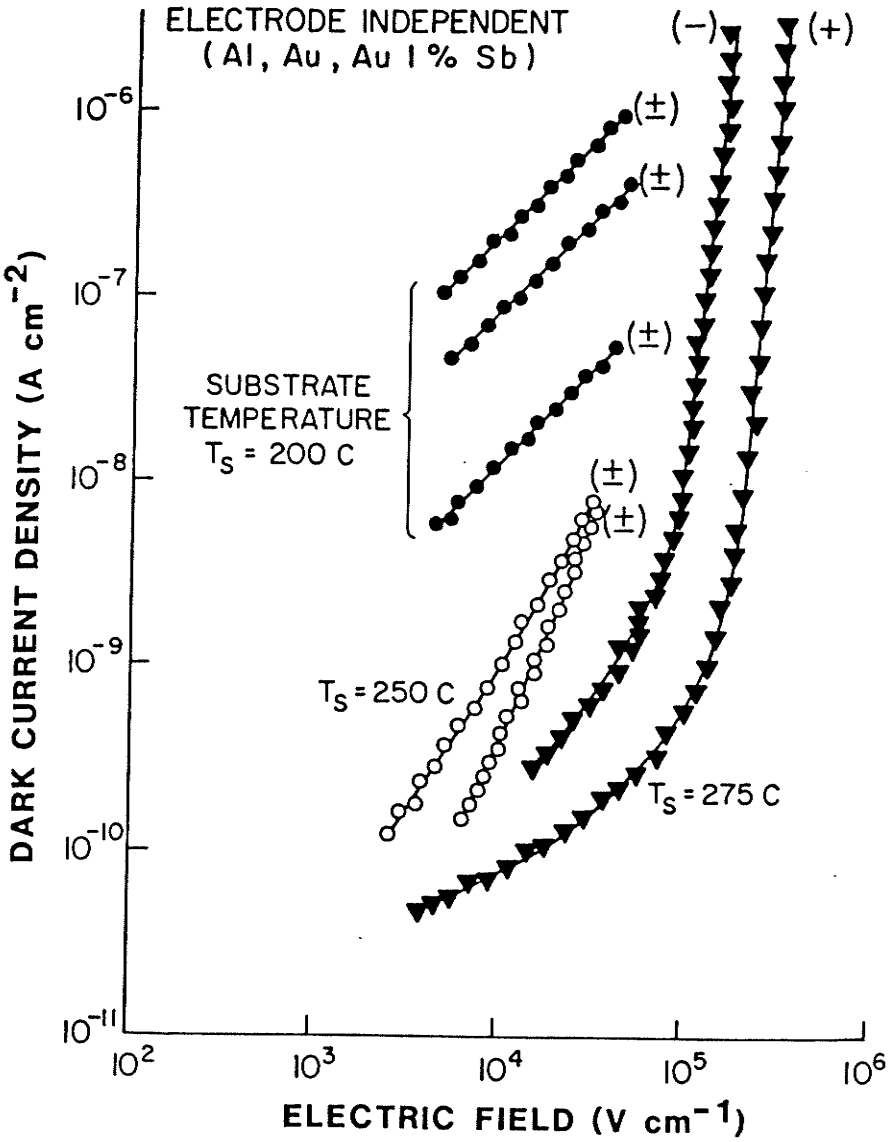

Figure 4.15: Dark conduction current vs. electric field.

tivity from 0.5 to 0.6 eV are attributed to variations in the oxygen content from film sample to film sample, which affects the energy distribution of midgap state density and hence the Fermi level.

One definite correlation , between the dark conductivity and the fabrication conditions in the chamber-discharge tube configuration, is that as the microwave power increases, the dark conduction current decreases, as shown in Table 4.2. It should be noted that all of these films contain appreciable oxygen contamination.

TABLE 4.2

Effect of the microwave power on dark conduction current.

P (W)	J* (A/cm)	Dep. rate (A/min)
400	5×10^{-10}	17
450	2×10^{-10}	5
510	8×10^{-11}	36
700	1.3×10^{-14}	29

* measured at an estimated electric field of 10^4 V/cm.

Table 4.2 shows that the deposition rate is not a monotonic function of the power. This is due to a very important parameter of this system which is the degree of invasion of the chamber by the plasma. In spite of using deposition parameters that are not equal, we can still see the effect of input microwave power upon the dark conductivity. From Table 4.2, it is clear that a high power level tends to increase

the sputtering of the discharge tube and the oxygen incorporation in the films, and in turn, to reduce the dark conductivity.

Photoconductivity. The photoconductivity can yield information concerning trapping and recombination centers, but often the interpretation is ambiguous. The photoconductivity of the a-Si:H films prepared using the discharge tube-chamber configuration is in general low. It increases with decreasing substrate temperature T_s. Since the dark conductivity also increases with decreasing temperature, it is more instructive to plot σ_{ph}/σ_d, the ratio of photoconductivity to dark conductivity, as it is shown in Fig. 4.16. From this figure it can also be seen that this ratio also increases with decreasing T_s (and thereby with decreasing oxygen content). This indicates that the photoconductivity is more sensitive to the oxygen contamination than the dark conductivity. In the next section we will be able to compare the data from Fig. 4.16, with photoconductivity of films produced by the short-circuited waveguide chamber configuration.

From the optical and electronic properties of the films prepared by the discharge tube-chamber configuration, it can be concluded that:

1. There is a high concentration of oxygen incorporated in the deposited films.

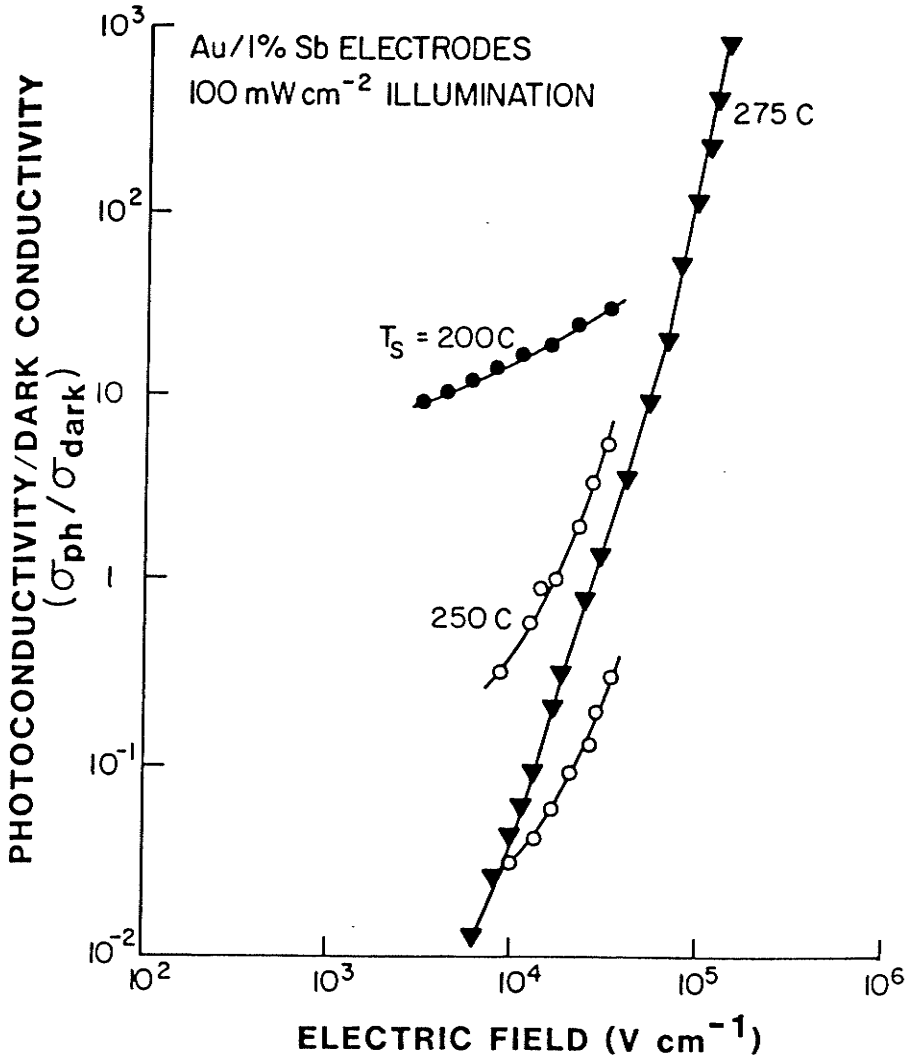

Figure 4.16: Photoconductivity to dark conductivity ratio.

2. The oxygen originated from the sputtering of the discharge tube.
3. The oxygen renders the deposited films insensitive to many of the deposition parameters.
4. This configuration limits the range of the deposition parameters.
5. The microwave power level required for deposition and the radiated power made the system unsafe for the operators.
6. The sputtering of the discharge tube represented a "fundamental limitation" for this system configuration, for the fabrication of semiconductor thin films.

4.4 SHORT-CIRCUITED WAVEGUIDE CHAMBER CONFIGURATION.

4.4.1 Experimental conditions

An axial dc magnetic field was applied to the waveguide chamber by means of an external coaxial coil; the coil current was varied over the range 0-22 A, which resulted in magnetic field strengths in the range 0 to 300 gauss, and with profiles as shown in Fig. 4.17 . Substrates mounted with their surface parallel and normal to the electric field were used to produce V-type samples and H-type samples.

The deposition rate profile along the axis of the waveguide chamber is dependent upon the dc magnetic field profile employed during the deposition, and it was generally

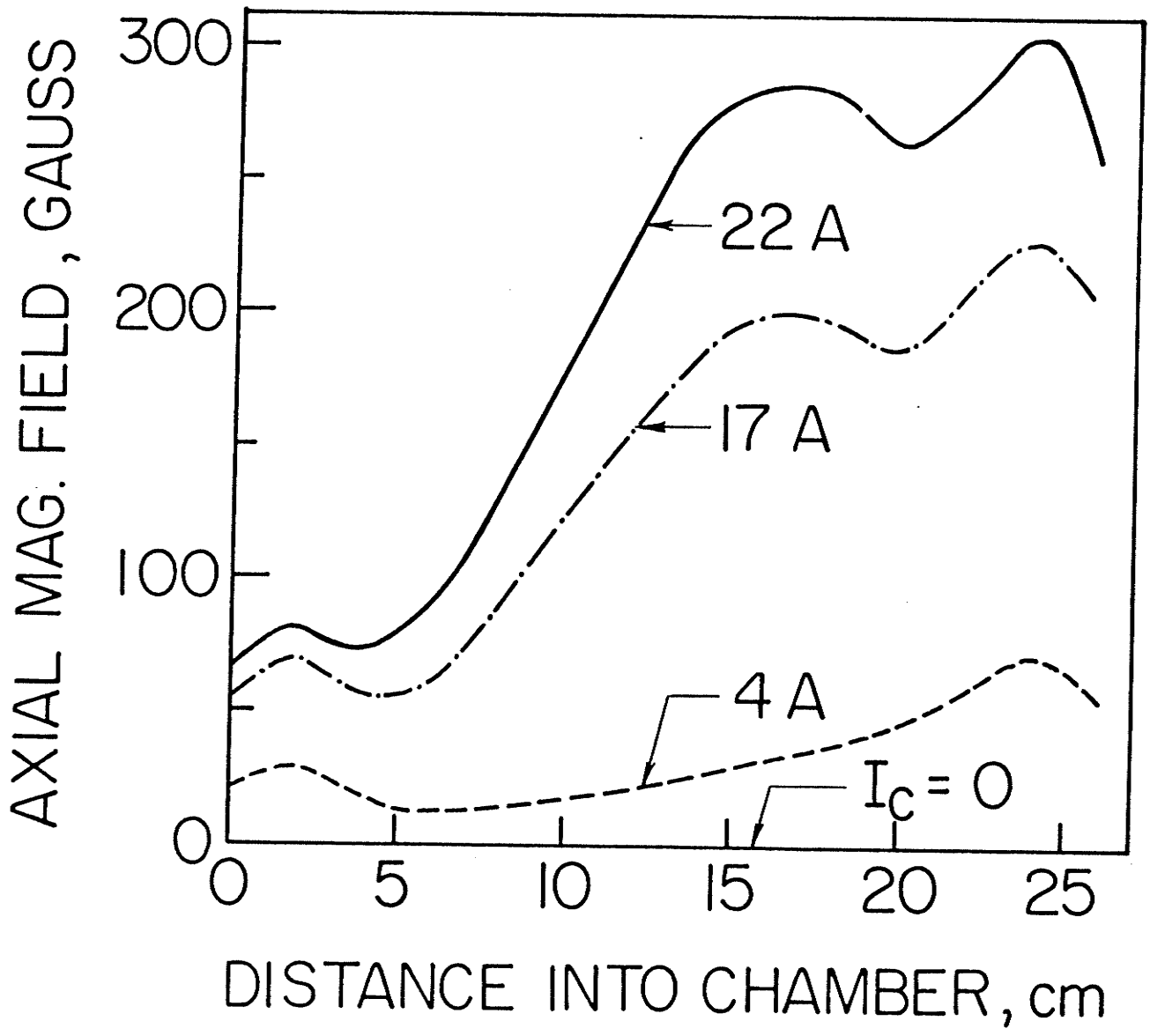

Figure 4.17: Magnetic field profile for various coil currents.

higher, by a factor of two, for the H-type sample, compared to the V-type sample. Figure 4.18 shows the deposition rate along the axis of the waveguide chamber for both type of samples, and for each of the magnetic field profiles shown in Fig. 4.17. It is apparent from Fig. 4.18 that the focus of deposition shifts away from the entrance of the waveguide chamber as the magnetic field increases. This is particularly so for the deposition rate profile corresponding to the 22 A coil current. From a practical point of view, this shift is very important because it reduces, or eliminates, thin film deposition on the entrance window. It should be remembered that a similar problem with the chamber-discharge tube configuration was the cause of instabilities of the deposition conditions, and that a thick film gradually deposited on the discharge tube bringing the deposition process to an end. A second effect of the magnetic field is to broaden the deposition rate profile for the H-type samples, as shown by the curve for the 22 A coil current.

OES of the plasma was conducted during the deposition of the films. Emission from plasma components (intensity of the SiH band, H_α , Ar), including emission from possible impurities such as copper and oxygen, were monitored; these impurities were not observed for the operating conditions employed. X-ray microanalysis of the deposited films also revealed no observable impurities.

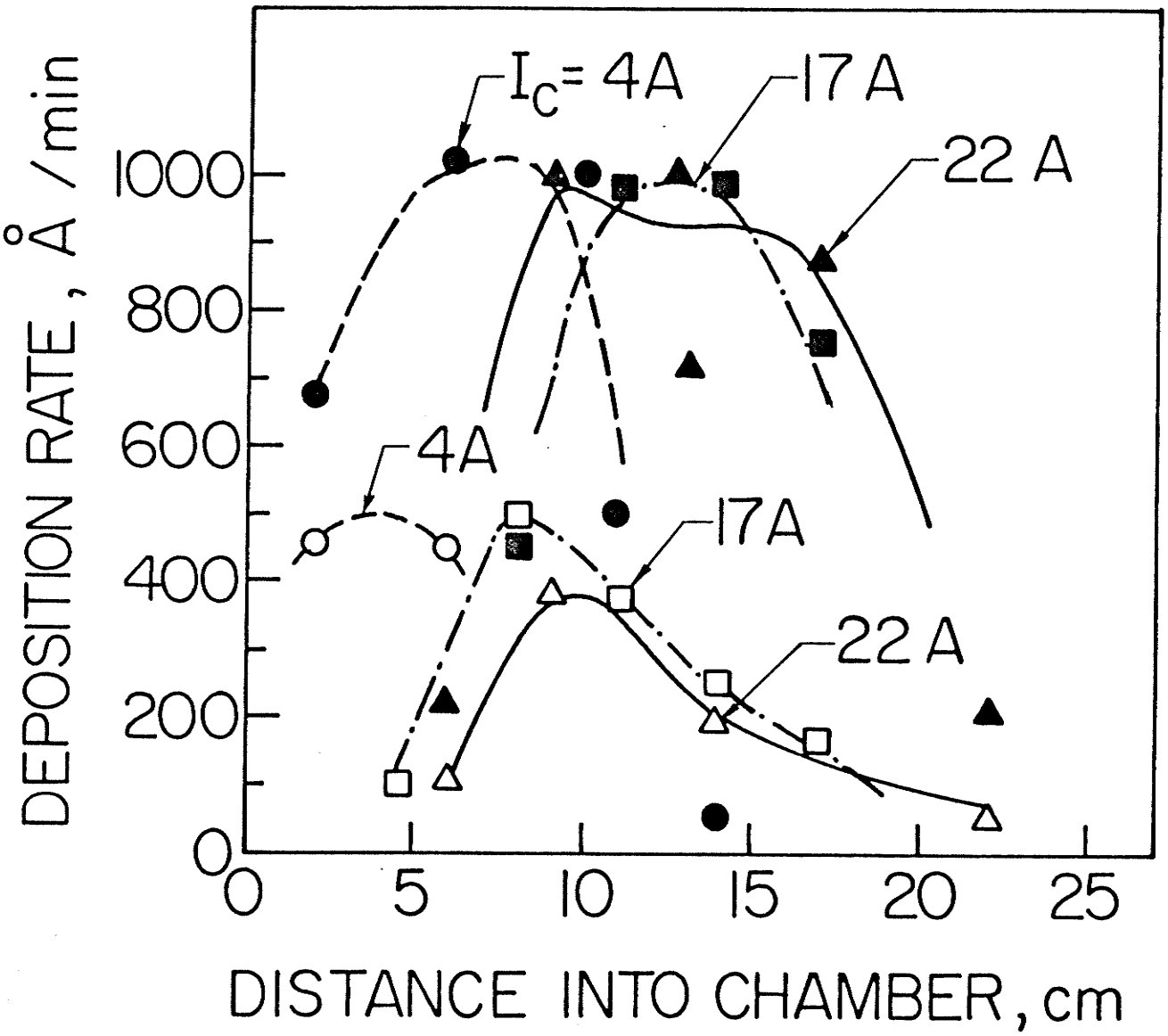

Figure 4.18: Deposition rates along the chamber.

The film characterization techniques, of which details have been given in section 4.1, were SEM, x-ray diffraction, IR and visible spectrophotometry, conductivity, and photoconductivity. Samples mounted horizontally (H) consistently exhibited a columnar growth structure as shown in Fig. 4.6, whereas no columnar structure was observed for vertically (V) mounted samples. All films were amorphous.

For the results presented in this section, the following deposition conditions were employed:

1. Gas composition: 10% silane, 45% hydrogen, and 45% argon.
2. Total flow rate: 30 sccm.
3. Microwave power: 45 W.
4. Pressure: 0.1 torr.
5. Substrate temperature: 200 °C.

The optical gap E_o is consistently 0.05 eV larger for the V samples than for H samples. A similar trend is also observed for the B value. Typical values for E_o and B are 1.7 eV and 4 x 10^5 $cm^{-1}eV^{-1}$, respectively.

Figure 4.19 shows the typical dependence of the dark conductivity and the photoconductivity of the a-Si:H films upon the axial magnetic field (coil current), for both V and H samples. The ratio of the photoconductivity to the dark conductivity was larger for V samples than for H samples, in the best cases (not shown) attaining a value of more than three orders of magnitude.

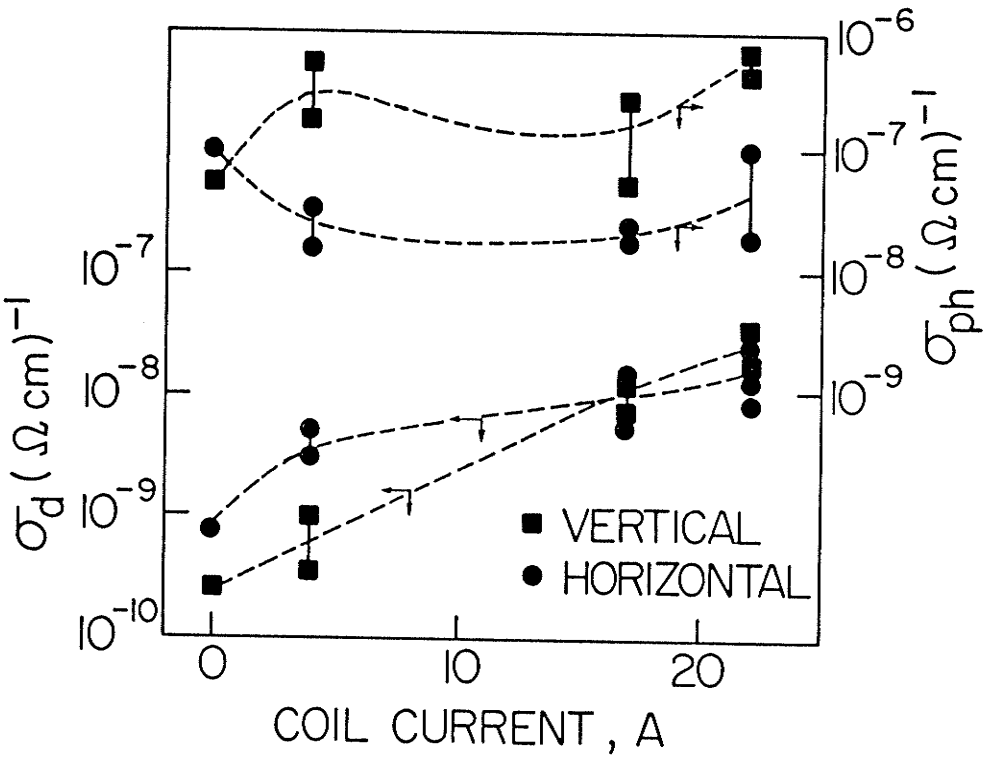

Figure 4.19: Dark conductivity and photoconductivity of a-Si:H.

A typical infrared spectrum is shown in Fig. 4.20. Pronounced absorption at 2000 and 2090 cm^{-1} are observed. Since peaks of absorption at 890 and 845 cm^{-1} are also observed, we interpret the absorption at 2090 cm^{-1} as a stretch mode of an $(SiH_2)_n$ chain [26], and the absorption at 2000 cm^{-1} as the stretch mode of SiH bonds. These absorptions at 2000 and 2090 cm^{-1} are enhanced by the magnetic field, as it is shown in Fig. 4.21.

We have also observed a higher degree of hydrogen incorporation in the H samples. On the basis of our other observations we conclude that this is associated with the columnar structure. It should be noted that a high dihydride concentration has been associated with the presence of argon in the gas mixture [41], and that high dihydride concentration reduces the quantum efficiency of photoconductivity and photoluminescence. Amorphous silicon produced with substrate temperatures from 25 to about 200 °C is known to develop strong dihydride absorptions [46]. Infrared measurements have revealed that films containing a high proportion of $(SiH_2)_n$ that are exposed to the atmosphere, also develop Si-O absorption after exposure time of days [23]. Dihydride chains are believed to be associated with voids, especially with the columnar growth observed in a-Si:H.

We have fabricated many hydrogenated amorphous silicon films by MPCVD using this system. The optical, electrical, and morphological properties of this material are very simi-

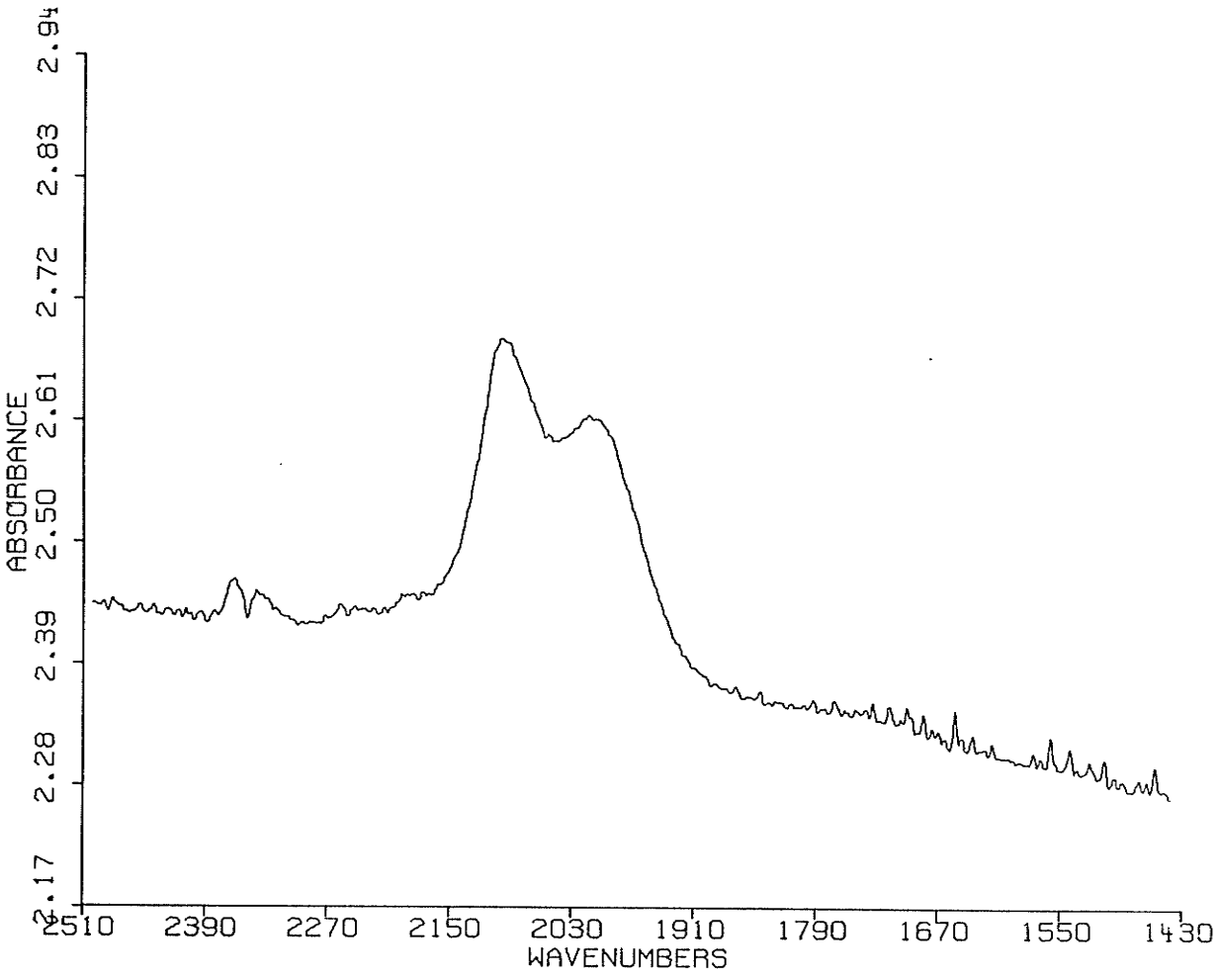

Figure 4.20: Typical infrared spectrum of an H-type a-Si:H film.

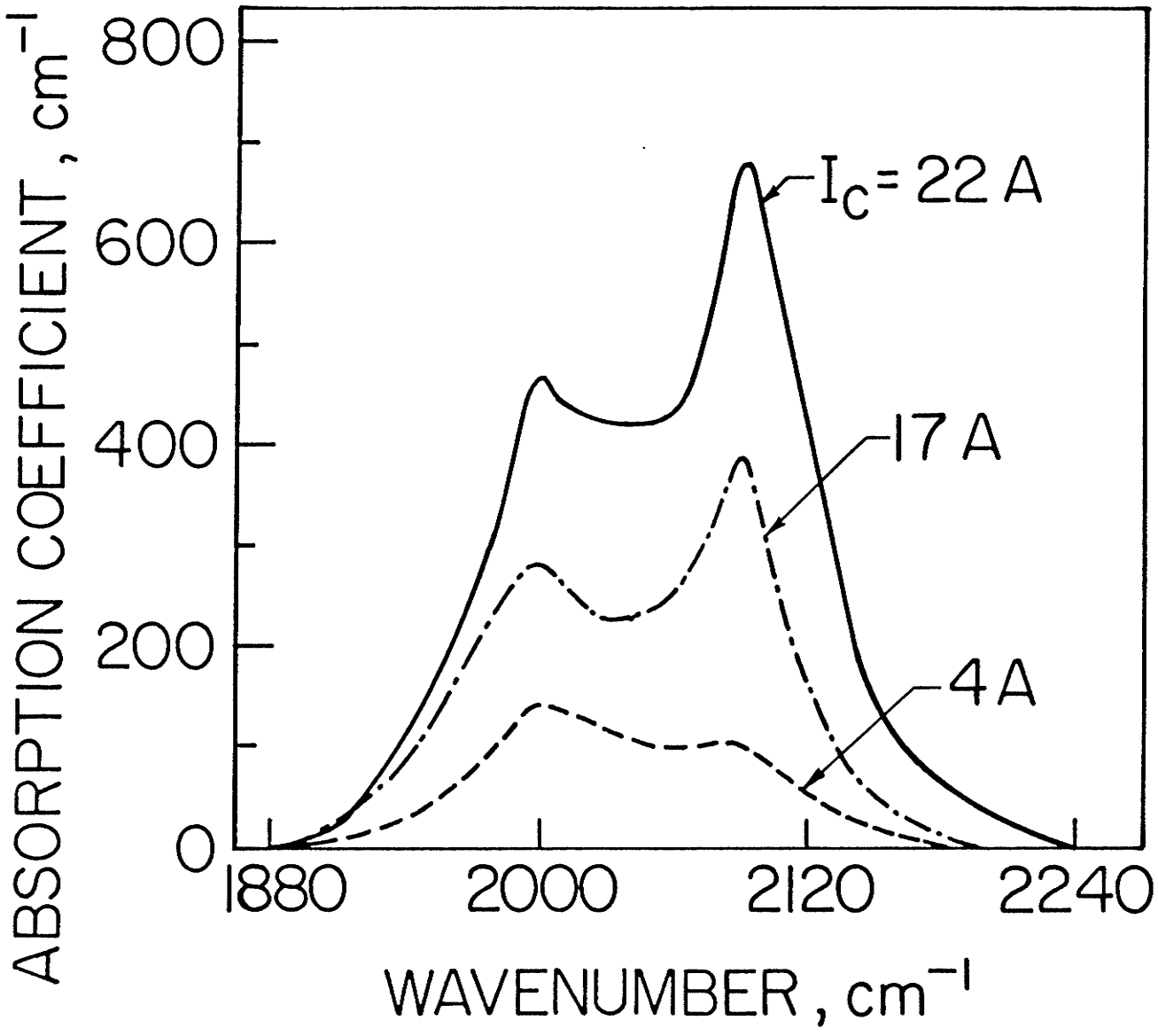

Figure 4.21: IR absorption of films vs. magnetic field confinement.

lar to that of the a-Si:H films prepared by the conventional dc or rf glow discharge techniques. We believe that the quality of the microwave a-Si:H films may be further improved by optimization of the deposition conditions.

Chapter V

CONCLUSIONS AND FUTURE WORK.

A prototype microwave plasma chemical vapour deposition system for the fabrication of amorphous semiconducting materials has been built and tested. Amorphous silicon-hydrogen alloys have been fabricated with a quality that is comparable to that of films fabricated by other techniques. Various contaminants of the deposited films have been detected, traced to their sources, and by changing configurations and designs, eliminated. In the process, microwave plasmas have manifested themselves as being very efficient in dissociating molecular gases, such as silane, and in sputtering the surrounding structures. In order to avoid bombardment of the chamber walls, the plasma has been confined by an axial dc magnetic field. This magnetic field has become not only a valuable means of avoiding contamination, but has removed a limitation encountered in other configurations by preventing the deposition of films at the microwave coupling window. Many questions about the plasma process, the film growth mechanism, and the relationship between these phenomena and the optical, electrical, and morphological properties of the films remain unanswered. Perhaps the principal one is the effect of the frequency of the electromagnetic excitation on

the film properties. The main objective was however accomplished: the feasibility of fabricating a-Si:H alloy films by microwave plasma CVD has been established. From the process of solving small problems and "fundamental limitations", a very flexible system is emerging. Since the confining magnetic field has been shown to influence the properties of the deposited samples, as well as the plasma chemistry, it has added one more degree of flexibility to an already flexible plasma process.

Further work is required in order to fully understand the microwave plasma CVD processes. However, two powerful techniques will help with this task: Optical Emission Spectrometry and Mass Spectrometry of the plasma. Any new work should be directed in three directions simultaneously: First, the prototype system has to be developed to a high quality system capable of holding high vacuum, with a controllable magnetic field, both in strength and profile. Secondly, a better understanding of the plasma is required so that a relation can be found between the plasma physics and the thin film growth process; and third, extended characterization techniques for the amorphous semiconductor thin films should be developed so that novel applications of the materials may be found.

A few steps along these directions have already been taken: A stainless steel waveguide chamber designed to withstand baking temperatures up to 400 °C, is being built,

a multipole magnetic coil is being designed in order to make the magnetic field profile along the axis of the chamber variable and to increase its field strengths up to 1000 gauss. A liquid nitrogen trap will be used to prevent oil vapours from backstreaming to the deposition chamber and to trap corrosive gases before they enter the pump. A high quality scanning monochromator and a control unit that can store wavelength and light intensity data, and can also be interfaced with a computer will be used for Optical Emission Spectroscopy of the plasma. The light detector will also be improved: instead of the silicon solar cell type detector that is now in use, an EMI photomultiplier with a quartz window, and a high quality high voltage power supply and current amplifier will be used. Furthermore, a partial pressure gauge, with a differential pumping system and a small aperture will be employed in order to gather more information about the reactive radicals in the plasma. Finally, characterization techniques such as luminescence and field effect measurements will be implemented. It is hoped that these studies will shed light upon the distribution of the density of states in the gap and in the band tails, and their effects on carrier transport in a-Si:H materials.

REFERENCES.

1. H. Adachi and K.C. Kao, "Dispersive optical constants of amorphous $Se_{1-x}Te_x$ films", J. Appl. Phys., Vol. 51, pp. 6326-6331, 1980.

2. W.P. Allis and D.J. Rose, "The Transition from Free to Ambipolar Diffusion", Phys. Rev., Vol. 93, pp. 84-91, 1954.

3. R.M.A. Azzam and N.M. Bashara, "Elipsometry and polarized light", North Holland, Amsterdam, 1977.

4. S.K. Bahl and S.M. Bhagat, "Properties of amorphous silicon film- dependence on deposition conditions", J. Non-Cryst. Solids, Vol. 17, pp. 409-427, 1975.

5. S.K. Bahl, S.M. Bhagat, and R. Glosser, "Properties of amorphous silicon films: dependence on deposition rate", Solid State Communications, Vol. 13, pp. 1159-1163, 1973.

6. A. Barna, P.B. Barna, G. Radnoczi, H. Sugawarw, and P. Thomas, "Computer simulation of the post-nucleation growth of thin amorphous germanium films", Thin Solid Films, Vol. 48, pp. 163-174, 1978.

7. S.C. Brown, "Introduction to Electrical Discharges in Gases", Ed. Wiley, New York, 1966.

8. D.E. Carlson and C.R. Wronski, "Amorphous Semiconductors", M.H. Brodski, editor, Springer-Verlag, New York, Chapter 10, 287, 1979.

9. J.F. Currie, P. Depelsenaire, J.P. Huot, L. Paquin, M.R. Wertheimer, "Compositional characterization of microwave plasma a-Si:H films", and A. Yelon, Can. J. Phys., Vol. 61, pp. 582-590, 1983.

10. E.C. Freeman and W. Paul, "Infrared vibrational spectra of rf-sputtered hydrogenated amorphous silicon", Physical Review B, Vol. 18, pp. 4288-4300, 1978.

11. E.C. Freeman and W. Paul, "Optical constants of rf sputtered hydrogenated amrphous Si", Physical Review B, Vol. 20, pp. 716-728, 1979.

12. R.R. Gay, D.L. Morel, D.P. Tanner, D. Kanani, and H.S. Ullal, "The effect of glow discharge excitation frequency on the performance of microcrystalline Si:H thin films and devices", Fourth European Conf. on Photovoltaic Solar Energy, page 714, Italy, 1982.

13. H. Fritzche, C.C. Tsai, and P. Persans "Amorphous semiconducting silicon-hydrogen alloys", Solid State Technology, pp. 55-60, January 1978.

14. T. Hamasaki, M. Ueda, M. Hirose, Y. Osaka, "Growth kinetics of amorphous hydrogenated silicon studied by pulsed rf discharge", Tenth Int. Conf. on Amorphous and Liquid Semiconductors, Tokyo, August 1983.

15. M.A. Heald, C.B. Wharton, "Plasma diagnostics with microwaves", John Wiley & Sons Inc., New York, 1965.

16. M. Hirose, M. Taniguchi, T. Nakashita, Y. Osaka, T. Susuki, S. Hasegawa, and T. Shimizu, "Defect compensation in doped CVD amorphous silicon", J. Non-Cryst. Solids Vol. 35&36, pp. 297-302, 1980.

17. J.R. Hollahan and A.T. Bell, eds. "Techniques and Applications of Plasma Chemistry", Wiley (Interscience), New York, 1974.

18. I. Kato, H.C. Card, K.C. Kao, S.R. Mejia, and L.Chow, "Microwave sputtering system for the fabrication of thin solid films", Rev. Sci. Instrum. Vol. 53, pp. 214-216, 1982.

19. I. Kato, H. Tsuchida, M. Nagai, "Radial distribution of excited atoms in a new coaxial line type microwave cw discharge tube", J. Appl. Phys. Vol. 51, pp. 5312-5315, 1980.

20. I. Kato, S. Wakana, S. Hara, "Microwave Plasma CVD System to Fabricate a-Si Thin Films out of Plasma", Jap. J. Appl. Phys., Vol. 22, pp. L40-L43, 1983.

21. I. Kato, S. Wakana, S. Hara, H. Kezuka, "Microwave Plasma CVD System for the Fabrication of Thin Solid Films", Jap. J. Appl. Phys., Vol. 21, pp. L470-L472, 1982.

22. J.C. Knights, "Nature of defects in plasma deposited a-Si:H films", J. Non-Cryst. Solids , Vol, 35&36, pp. 159-170, 1980.

23. J.C. Knights, G. Lucovsky, and R.J. Nemanich, "Defects in plasma-deposited a-Si:H", J. of Non-Cryst. Solids, Vol. 32, pp. 393-403, 1979.

24. J.C. Knights, R.A. Street, and G. Lucovsky, "Electronic and structural properties of plasma-deposited a-Si:O:H. The story of O_2", J. of Non-Cryst. Solids, Vol. 35&36, pp. 279-284, 1980.

25. P. Kocian, "Influence of the plasma parameters on the properties of a-Si films prepared by glow-discharge deposition method", J. Non-Cryst. Solids , Vol. 35&36, pp. 195-200, 1980.

26. G. Lucovsky, R.J. Nemanish, and J.C. Knights, "Structural interpretation of the vibrational spectra of a-Si:H alloys", Phys. Review B, Vol. 19, pp. 2064-2073, 1979.

27. G. Lucovsky, J. Yang, S.S. Chao, J.E. Tyler, and W. Czubatyj, "Oxygen-bonding enviroments in glow discharge-deposited amorphous silicon-hydrogen alloy films", Phys. Review B, Vol. 28, pp. 3225-3233, 1983.

28. A.D. Mac Donald, S.J. Tetenbaum, "High Frequency and Microwave Discharges", in Gaseous Electronics, Vol.1, pp. 173-217 (M.N. Hirsh, H.J. Oskam, eds.), Academic Press, New York, 1978.

29. M.S. Mathur, H.C. Card, K.C. Kao, S.R. Mejia, and G.C. Tabisz, "Far infrared spectra of amorphous-Si:H thin films on polyethylene", Canadian Journal of Physics, Vol. 61, pp. 305-308, 1983.

30. E.L. Mc Cracken, "Fortran program for analysis of ellipsometer measurements", Nat. Bur. Stds. Tech. note 479, Washington, D.C., 1969.

31. F.K. Mc Taggart, "Plasma Chemistry in Electrical Discharges", Elsevier Publishing Co., 1967.

32. S.R. Mejia, R.D. McLeod, K.C.Kao, and H.C. Card "The effects of deposition parameters on a-Si:H films fabricated by microwave glow discharge techniques", Tenth Int. Conf. on Amorphous and Liquid Semiconductors. Tokyo, August 1983.

33. N.F. Mott and E.A. Davis "Electronic Processes in Non-Crystalline Materials", Second Edition, Claredon Press, Oxford, 1979.

34. W. Paul, A.J. Lewis, G.A.N. Connel, and T.D. Moustakas, "Doping, Schottky Barrier and p-n Junction Formation in Amorphous Germanium and Silicon by rf Sputtering", Solid State Communications, Vol. 20, pp. 969-972, 1976.

35. R.C. Ross and R. Messier, "Microstructure and properties of rf-sputtered amorphous hydrogenated silicon films", J. Appl. Phys., Vol. 52, pp. 5329-5339, 1981.

36. I. Sakata, Y. Hayashi, M. Yamanaka, and H. Karasawa, "A new characterization parameter for hydrogenated amorphous silicon: B (the square of the gradient of the $(\alpha\hbar\nu)^{1/2}$ versus $\hbar\nu$ plot)", J. Appl. Phys., Vol. 52, pp. 4334-4336, 1981.

37. T.M. Shaw, "Dissociation of Hydrogen in a Microwave Discharge", J. Chem. Phys., Vol. 30, pp. 1366-1367, 1959.

38. T. Shimizu, M. Kumeda, I. Watanabe, K. Kamono, "Influence of oxygen and deposition conditions on sputtered a-Si", J. Non-Cryst. Solids, Vol. 35&36, pp. 303-308, 1980.

39. W.E. Spear and P.G. Le Comber, "Electronic properties of substitutionally doped amorphous Si and Ge", Phil. Mag. Vol. 33, pp. 935-949, 1976.

40. S.M. Sze, "Physics of Semiconductor Devices", Second Edition, Wiley, New York, Chap. 5, 1981.

41. K. Tanaka, S.Yamasaki, K. Nakagawa, A. Matsuda, H. Okushi, M. Matsumura, and S.Iizima, "The role of argon involved in plasma-deposited amorphous Si:H films." J. of Non-Cryst. Solids, Vol. 35&36, pp. 475-480, 1980.

42. M. Taniguchi, M. Hirose, and Y. Osaka, "Substitutional doping of chemically vapor-deposited amorphous silicon", J. Crystal. Growth Vol. 45, pp. 126-131, 1978.

43. J. Tauc, "Amorphous and liquid semiconductors", Plenum Press, New York, 1974.

44. J.L. Vossen, J.J. Cuomo, "Glow discharge sputter deposition", in Thin Film Processes, Ed. by J.L. Vossen and W. Kern, Academic Press, New York, 1978.

45. H. Yasuda and T. Hsu "Some Aspects of Plasma Polymerization Investigated by Pulsed R.F. Discharge", J. Polym. Sci. Polym. Chem. Ed., Vol. 15, pp. 81-97, 1977.

46. P.J. Zanzucchi, C.R. Wronski, and D.E. Carlson, "Optical and photoconductivity properties of discharge produced amorphous silicon", J. Appl. Phys., Vol. 48, pp. 5227-5236.